

# Iron-responsive element of Divalent metal transporter 1 (Dmt1) controls Notch-mediated cell fates

Judith Hounjet<sup>1</sup>, Arjan J. Groot<sup>1</sup>, Jolanda P. Piepers<sup>1</sup>, Onno Kranenburg<sup>2</sup>, Danny A. Zwijnenburg<sup>3</sup>, Francesca A. Rapino<sup>1,4</sup>, Jan B. Koster<sup>3</sup>, Kim R. Kampen<sup>1</sup>  and Marc A. Vooijs<sup>1</sup> 

<sup>1</sup> Department of Radiation Oncology (Maastr), GROW School for Oncology, Maastricht University Medical Centre+, Maastricht, The Netherlands

<sup>2</sup> Lab Translational Oncology, Division Imaging and Cancer, University Medical Center Utrecht, The Netherlands

<sup>3</sup> Center for Experimental and Molecular Medicine, Amsterdam UMC Location University of Amsterdam, The Netherlands

<sup>4</sup> Department of Pharmacy, Giga Stem Cells, University of Liege, Belgium

## Keywords

divalent metal transporter 1 (Dmt1, Slc11A2, NRAMP2); iron; notch; stem cell fate and differentiation; vesicles

## Correspondence

M. A. Vooijs, Department of Radiation Oncology (Maastr), GROW School for Oncology, Maastricht University Medical Centre+, Postbox 616, 6200 MD, Maastricht, The Netherlands  
 Tel: +31 (0)43 3882912  
 E-mail: [marc.vooijs@maastrichtuniversity.nl](mailto:marc.vooijs@maastrichtuniversity.nl)

Judith Hounjet and Arjan J. Groot contributed equally to this article

(Received 14 February 2023, revised 12 July 2023, accepted 29 August 2023)

doi:10.1111/febs.16946

Notch receptor activation is regulated by the intramembrane protease  $\gamma$ -secretase, which cleaves and liberates the Notch intracellular domain (Nidc) that regulates gene transcription. While  $\gamma$ -secretase cleavage is necessary, we demonstrate it is insufficient for Notch activation and requires vesicular trafficking. Here, we report Divalent metal transporter 1 (Dmt1, Slc11A2) as a novel and essential regulator of Notch signalling. Dmt1-deficient cells are defective in Notch signalling and have perturbed endolysosomal trafficking and function. Dmt1 encodes for two isoforms, with and without an iron response element (ire). We show that isoform-specific silencing of Dmt1-ire and Dmt1+ire has opposite consequences on Notch-dependent cell fates in cell lines and intestinal organoids. Loss of Dmt1-ire suppresses Notch activation and promotes differentiation, whereas loss of Dmt1+ire causes Notch activation and maintains stem-progenitor cell fates. Dmt1 isoform expression correlates with Notch and Wnt signalling in Apc-deficient intestinal organoids and human colorectal cancers. Consistently, Dmt1-ire silencing induces Notch-dependent differentiation in colorectal cancer cells. These data identify Dmt1 isoforms as binary switches controlling Notch cell fate decisions in normal and tumour cells.

## Introduction

Notch signalling constitutes a highly conserved pathway in tissue homeostasis that occurs during development and in adult tissues [1]. Notch receptors are transmembrane transcriptional regulators that are activated by ligand-induced cleavage. In the absence of ligands, Notch receptors are in a proteolysis-resistant state. Upon ligand binding, the receptor unfolds and undergoes cleavage

through Adam10 protease at the S2-site (NEXT). Subsequent cleavage at the S3 site by  $\gamma$ -secretase releases the Notch intracellular domain (Nidc) that translocates to the nucleus. Together with the DNA binding protein RBP-jK, it activates Notch downstream target genes [2].

Aberrant Notch signalling is observed in many human malignancies, including T-ALL, breast ,

## Abbreviations

cAMP, cyclic-AMP; Dll4, delta-like 4; Dmt1, Divalent metal transporter 1; DOX, doxycycline; Eea1, early endosomal marker 1; GSI,  $\gamma$ -secretase inhibitor; Ire, iron-responsive element; Lamp1, lysosomal-associated membrane protein 1; Lc3b-II, microtubule-associated proteins 1A/1B light chain 3B-II; MEF, mouse embryonic fibroblasts; Msf, myosin skeletal FAST; Myf5, myogenic factor 5; MyoD, myoblast determination protein 1; MyoG, myogenin; NAC, n-acetyl cysteine; NEXT, S2-cleaved Notch1 receptor; Nidc, Notch intracellular domain; Rab5, Ras-related protein 5; ROS, reactive oxygen species; Slc11A2, solute carrier family 11, member 2; TfR1, transferrin receptor 1; TMIC, S1-cleaved Notch1 receptor; U9, screening cell line.

colorectal and lung cancer [3]. Unlike ligand-dependent Notch signalling, ligand-independent Notch signalling requires  $\gamma$ -secretase activity but is independent of Adam10 [4–7]. Notch/ $\gamma$ -secretase cleavage occurs at the cell surface and in the endosomes and lysosomes [8,9], differentially regulating Notch stability and transcriptional activity [10]. Recently, we demonstrated that Presenilin2-containing  $\gamma$ -secretase complexes localize to endosomes [11], and that increasing endosomal and lysosomal pH strongly inhibits oncogenic Notch signalling [12–16]. These findings indicate that endosomal and lysosomal trafficking plays an essential role in the ligand-independent processing of Notch1; however, an in-depth understanding of ligand-independent Notch signalling is lacking.

Here, we used a shRNA gene silencing screen to find new rate-limiting regulators of ligand-independent Notch signalling. We identified Divalent metal transporter 1 (Dmt1), a proton-coupled transmembrane transporter of  $\text{Fe}^{2+}$  and other divalent metals, as a novel Notch regulator [17]. Dmt1 mouse mutants are highly anaemic, indicating its essential role in intestinal iron absorption and metabolism [17–20]. Dmt1 is encoded by the *Slc11A2* (solute carrier family 11, member 2) gene that is expressed as four different transcript isoforms due to alternative promoter usage (*Dmt1a* and *Dmt1b*) and the presence or absence of an iron-responsive element (ire) in the 3'UTR [21–23]. Recent evidence suggests that despite all four isoforms exhibiting similar iron transport efficiency, they have distinct functions [23,24]. Furthermore, Dmt1 isoforms present organ specificity; *Dmt1a* is expressed only in the duodenum and kidney, whereas *Dmt1b* is ubiquitously expressed [22], suggesting that its function might differ in a cell-type-specific manner.

Here, we show that Dmt1 isoforms, with or without an iron-responsive element, oppositely regulate Notch signalling in various mammalian cell types. Specifically, silencing the *Dmt1-ire* isoform suppresses Notch activation and induces the differentiation of muscle, neural and normal intestinal epithelial cells, and colorectal cancer cells. Conversely, knockdown of *Dmt1+ire* results in Notch hyperactivation in the same cell types and induces stemness in mouse intestinal organoids. Furthermore, in intestinal organoids from Apc-mutant mice, and human colorectal cancer, Dmt1 isoform expression correlates with Notch activity. Thus, our study defines Dmt1 isoforms as novel checkpoints that dictate the fate of Notch receptor activity during intracellular transport to control cell renewal and differentiation in mammalian (cancer) cells and tissues.

## Results

### Loss of Dmt1 blocks Notch signalling

We and others have shown that ligand-dependent Notch signalling requires the Adam10 protease S2 cleavage step [7,25]. Therefore, we examined whether ligand-independent Notch signalling also requires Adam10 and the related Adam17. We transduced Adam10 and Adam17 knockout (Adam10<sup>-/-</sup>/17<sup>-/-</sup>) mouse embryonic fibroblasts (MEFs) with a Myc-tagged murine Notch1 cDNA that lacked ligand-binding EGF-like repeats and harboured the gain-of-function mutation found in human leukaemia's ( $\Delta$ EGF-Notch1-L1594P-6xMYC), rendering it ligand-independent [7]. These cells also express a GFP luciferase-driven Notch transcriptional reporter (12xCSL-GFP-Luciferase) and are referred to as the screening cell line (U9). We discovered Notch1 to be transcriptionally active in the U9 cells (Fig. 1A) and cleaved at the common S3-Val1744-cleavage site (Fig. 1B), despite the absence of both Adam10 and Adam17. Furthermore, Notch transcriptional activity and cleavage were blocked by the  $\gamma$ -secretase inhibitor DBZ (GSI), validating U9 cells as a faithful Notch reporter for  $\gamma$ -secretase-dependent Notch signalling. Consistent with our previous research, we found that the Notch1 activity in U9 cells was blocked entirely by the vesicle-targeting agents, chloroquine and Bafilomycin A1, despite cleaved Nid1 as shown previously (Fig. 1A,B) [12]. These data highlight that Adam10 and Adam17 are not required for ligand-independent Notch signalling, that  $\gamma$ -secretase cleavage is not sufficient for Notch transcriptional activity and that Notch trafficking in intracellular vesicles is rate-limiting.

To identify these unknown Notch regulators, we conducted a shRNA drop-out screen in U9 reporter cells (Fig. 1C, Fig. S1A). We identified more than 100 significant hits that strongly downregulated Notch reporter activity. *Cntnap1* and *Slc11a2* (Fig. 1D, Fig. S1B) showed the highest enrichment of sequence reads. Of note, *Cntnap1* is a known  $\gamma$ -secretase-associated protein-regulating Notch processing and activity [26,27], validating our screening platform. *Slc11a2* encodes for Divalent metal transporter 1 (Dmt1), a proton-coupled transmembrane protein responsible for the transport of iron ( $\text{Fe}^{2+}$ ) and other divalent metals [17]. In addition, pathway analysis revealed significant enrichment for (ion) transmembrane transporter and transition metal ion binding (Fig. 1E, Table S1). Subsequently, we created Dmt1 knockout (KO) MEFs that lack the Dmt1 protein from MEFs endogenously expressing Dmt1b-ire and

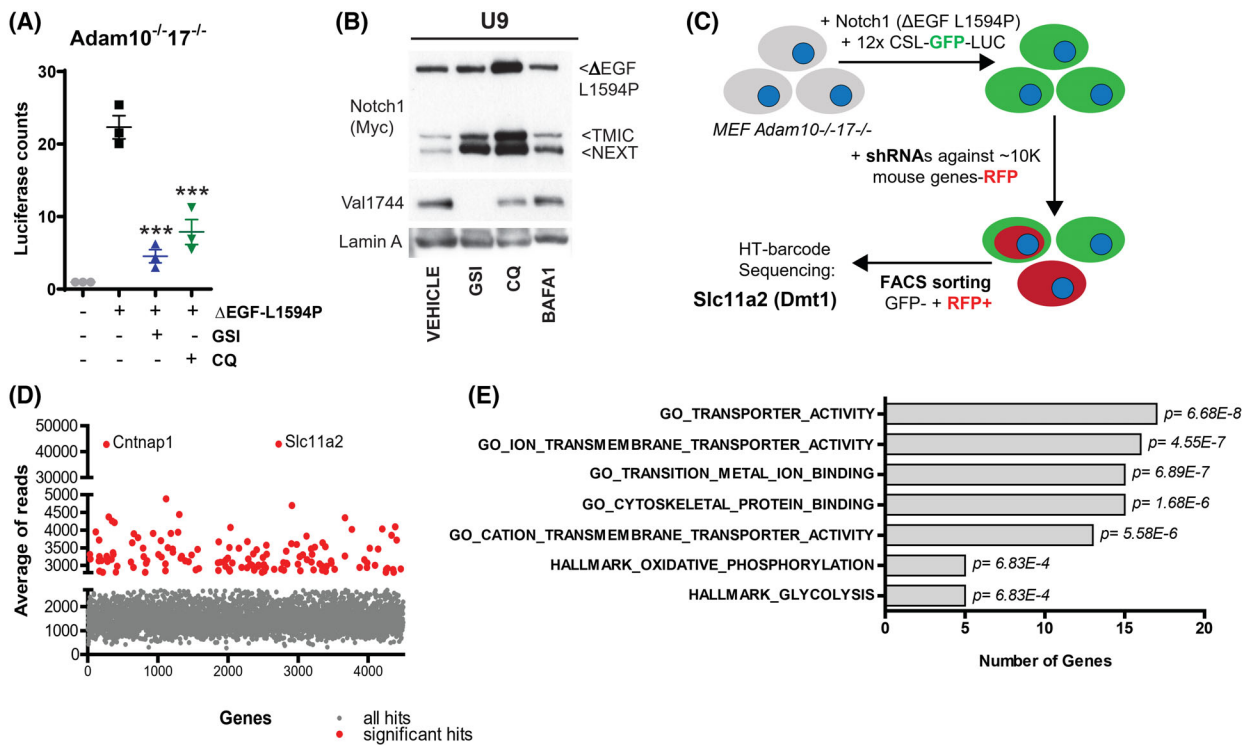


**Fig. 1.** Loss of Dmt1 inhibits ligand-independent Notch signalling. (A) Notch1 activity in a screening cell line (U9) upon  $\Delta$ EGF-Notch1-L1594P expression and DMSO, GSI or chloroquine (CQ) treatment for 24 h measured by luciferase counts [one-way ANOVA (Tukey comparison), \*\*\* $P < 0.001$ , significantly compared with control]. (B) Immunoblot analysis of (cleaved) Notch1 (Myc), Val1744 and  $\beta$ -Actin (loading control) in U9 cells treated with DMSO, GSI, chloroquine (CQ) or Bafilomycin A1 (BAFA1) for 24 h. Notch reporter for  $\gamma$ -secretase-dependent Notch signalling due to inhibition of Nid1 formation, as shown by the appearance of S2-cleaved Notch1 (Next). (C) shRNA screen in Adam10<sup>-/-17-/-</sup>-deficient MEFs expressing active ligand-independent Notch1 and Notch reporter. RFP-positive and GFP-null expressing cells were sorted, and HT-barcode sequencing revealed the Slc11a2 gene, encoding Dmt1 as a novel regulator of Notch signalling. (D) Representation of genes that were included in the shRNA screen. Nonsignificant (grey dot) and significant (red dot) genes are shown according to the average number of reads from the screen. (E) Pathway analysis of the shRNA screen reporting the number of genes included in each of the pathways. GSI,  $\gamma$ -secretase-inhibitor dibenzazepine. Data are representative of three independent experiments and values are expressed in mean  $\pm$  SD.

Dmt1b+ire (Fig. S1C,D). Functionally, Dmt1 KO MEFs showed reduced transport activity of the divalent metals Fe<sup>2+</sup> and Co<sup>2+</sup> (Fig. S1E) and reduced uptake of fluorescently labelled transferrin (Fig. S1F) without affecting the expression of transferrin receptor 1 (TfR1) (Fig. S1D). To investigate whether loss of Dmt1 affected endogenous Notch1 signalling, Dmt1 WT and KO MEFs were stimulated with Notch ligand (Dll4). In Dll4-stimulated Dmt1 WT MEFs, potent GSI-dependent activation of Notch targets *Hey1* and *Hey2* was observed (Fig. 2A). In contrast, neither Dll4 (Fig. 2A) nor Jagged2 (Fig. S2A) stimulation in Dmt1 KO MEFs led to expression of Notch targets *Hey1* or *Hey2*. Total *Notch1* receptor expression was similar between Dmt1 WT and KO MEFs (Fig. S2B).

To determine whether Dmt1 KO MEFs have a general defect in nuclear transport and transcriptional

activation, we overexpressed doxycycline-inducible Nid1. We observed that Nid1 expression (Fig. S2C), nuclear translocation (Fig. 2B) and *Hey1* mRNA expression (Fig. S2D) were similar between Dmt1 WT and KO MEFs. These findings demonstrate that loss of Dmt1 inhibits ligand-induced endogenous Notch signalling and acts upstream or parallel to Notch/ $\gamma$ -secretase cleavage that produces Nid.

### Dmt1 controls vesicular trafficking and clearance of cleaved Notch

Surprisingly, we observed increased levels of Val1744-cleaved Notch1 in Jagged2-stimulated Dmt1 KO MEFs (Fig. 3A), despite diminished *Hey1* expression (Fig. S2E), similar to perturbation of Notch signalling in cells by CQ and BafA1 (Fig. 1A,B). In addition, the

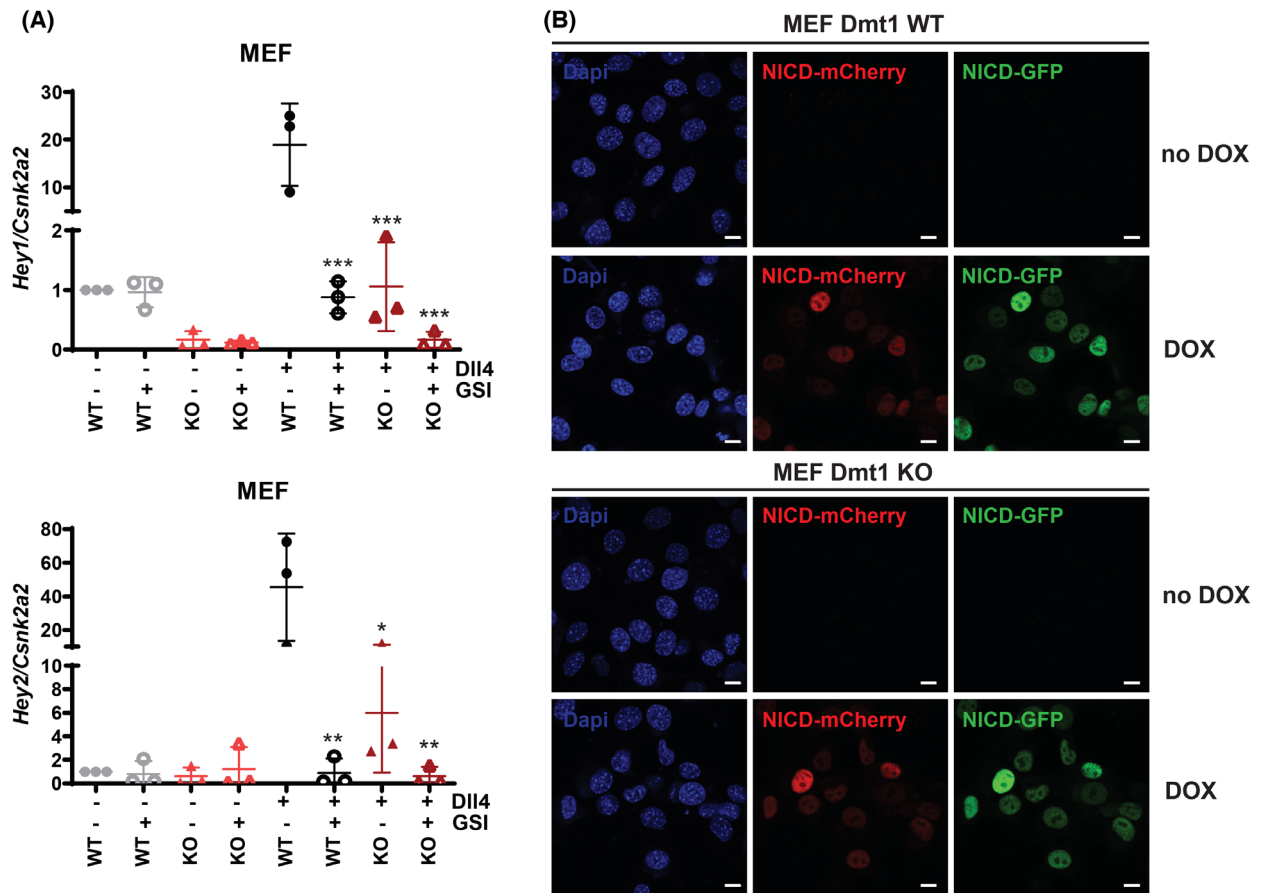
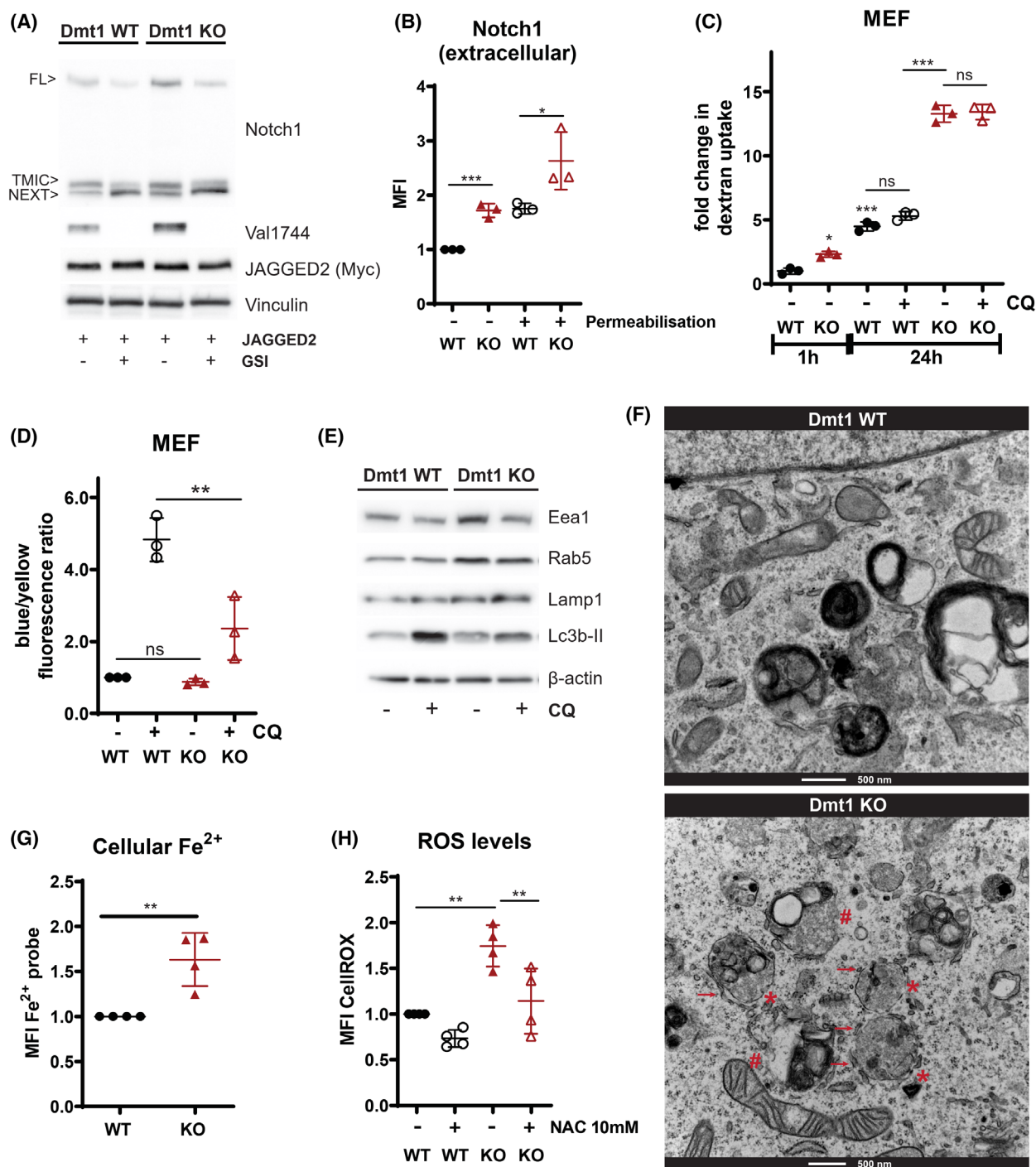


**Fig. 2.** Loss of Dmt1 results in diminished endogenous Notch1 signalling, which is rescued by overexpression of Nicd. (A) mRNA expression levels of Notch target genes, Hey1 and Hey2, in Dmt1 WT and KO MEFs stimulated with DII4 and treated with DMSO or GSI for 24 h, measured by qRT-PCR. Csnk2a2 mRNA expression was employed as a housekeeping control [one-way ANOVA (Tukey comparison),  $*P < 0.05$ ,  $**P < 0.01$ ,  $***P < 0.001$ , significantly compared with Dmt1 WT cells stimulated with DII4]. (B) Fluorescent ectopic expression of Nicd1-mCherryGFP in Dmt1 WT and KO cells upon doxycycline (DOX)-induction. Cells were counterstained with DAPI. Scale bar: 10  $\mu$ m. GSI,  $\gamma$ -secretase inhibitor dibenzazepine. Data are representative of three independent experiments, and values are expressed in mean  $\pm$  SD.

**Fig. 3.** Loss of Dmt1 results in increased Notch1 cleavage and disturbed intracellular trafficking. (A) Immunoblot analysis of Notch1 (C-20), Val1744, Myc (JAGGED2) and Vinculin (loading control) protein levels in Dmt1 WT and KO MEFs treated with DMSO or GSI for 24 h. (B) Flow cytometry analysis of extracellular Notch1 receptor expression at the plasma membrane (unpermeabilized) and total expression (permeabilized) in Dmt1 WT and KO MEFs (Student *t*-test,  $*P < 0.05$ ,  $***P < 0.001$ ). (C) Fluorescently labelled dextran uptake within 1 and 24 h in Dmt1 WT and KO MEFs, pretreated with or without chloroquine for 24 h, measured by flow cytometry (one-way ANOVA [Tukey comparison], ns, nonsignificant,  $*P < 0.05$ ,  $***P < 0.001$ , significantly compared with untreated Dmt1 WT MEFs after 1 h of dextran uptake). (D) Blue/yellow fluorescence ratio of Dmt1 WT and KO MEFs pretreated with or without chloroquine for 24 h, after 24 h of Lysosensor-labelled dextran uptake [one-way ANOVA (Tukey comparison), ns, nonsignificant,  $**P < 0.01$ , significantly compared with untreated Dmt1 WT MEFs]. (E) Immunoblot analysis of Eea1, Rab5, Lamp1, Lc3b-II and  $\beta$ -Actin (loading control) protein levels in Dmt1 WT and KO MEFs treated with or without chloroquine for 24 h. (F) Representative electron microscopy images of Dmt1 WT and KO MEFs. Dmt1 KO MEFs show damaged intracellular vesicles, displaying nonintact membranes (red asterisks), missing membranes (red hashtags) and formation of isolation membranes (phagophores, red arrows). (G) Cellular  $Fe^{2+}$  probe fluorescence in Dmt1 WT and KO MEFs measured by flow cytometry (Student *t*-test,  $**P < 0.01$ ). (H) Cytoplasmic ROS levels measured by flow cytometry in Dmt1 WT and KO MEFs (pretreated with 10 mM of NAC; one-way ANOVA [Tukey comparison],  $**P < 0.01$ ). CQ, chloroquine; Eea1, Early endosome antigen-1; GSI,  $\gamma$ -secretase-inhibitor dibenzazepine; Lamp1, lysosomal-associated membrane protein 1; Lc3b-II, membrane-associated microtubule-associated protein 1 light chain 3-II; MFI, median fluorescent intensity; NAC, N-acetyl-L-cysteine. Data are representative of three independent experiments, and values are expressed in mean  $\pm$  SD.



full-length, S1-furin-cleaved (Tmic) and S2-cleaved (Next) Notch1 receptor levels were increased in Dmt1 KO MEFs. Total and cell surface staining for Notch1 demonstrated a twofold increase in the Notch1 receptor levels in Dmt1 KO MEFs, albeit without a change in the surface/total ratio (Fig. 3B).

Because we observed high levels of Val1744-cleaved Nid1 without target gene activation in Dmt1 KO cells, we investigated whether Dmt1 loss perturbs Notch1 receptor trafficking. We observed a threefold increase in the uptake of fluorescently labelled dextran within 24 h in Dmt1 KO MEFs compared with wild-

type cells, which was not affected by blocking autophagy with chloroquine (Fig. 3C). We utilized dextran as a pH sensor to test whether intracellular pH changes correlated perturbed Notch activity, using a dextran-emitting yellow fluorescence in acidic and blue fluorescence in neutral environments. In Dmt1 KO MEFs, an absolute increase in yellow and blue fluorescence was observed compared with the uptake in Dmt1 WT MEFs (Fig. 3C, Fig.S2F); however, the ratio remained constant (Fig. 3D). Chloroquine neutralized the pH (increase in blue fluorescence) in both Dmt1 wild-type and KO cells.

Furthermore, compared with Dmt1 WT MEFs, Dmt1 KO MEFs also exhibited increased levels of the early endosomal marker 1 (Eea1), Rab5, the lysosomal-associated membrane protein 1 (Lamp1) and the autophagosome marker Lc3b-II (Atg8) (Fig. 3E). In addition, we observed a decreased autophagic flux in Dmt1 KO MEFs, evident by the decreased accumulation of Lc3b-II in the presence of chloroquine. In line with this, electron microscopic analysis of Dmt1 KO MEFs revealed damaged intracellular vesicles with disrupted and punctured membranes (Fig. 3F). These data suggest that loss of Dmt1 compromises the integrity of endo/lysosomal membranes, disrupting the autophagy/lysophagy catabolic process and trafficking of Notch receptors.

To understand how Dmt1 loss perturbs vesicle integrity, we measured cytoplasmic  $\text{Fe}^{2+}$  and ROS levels as the cytotoxic by-products of iron-catalysed reactions upon deregulated metal transport. Dmt1 KO MEFs showed increased cellular levels of  $\text{Fe}^{2+}$  (Fig. 3G) and accumulation of cytoplasmic ROS, which could be reverted by the antioxidant n-acetyl cysteine (NAC) (Fig. 3H). Collectively, these data suggest that Dmt1 deficiency may cause vesicle membrane damage due to abnormal iron ( $\text{Fe}^{2+}$ ) accumulation and metabolism, leading to oxidative stress.

### Dmt1 iron response element controls Notch1 signalling differentially

Dmt1 occurs in different isoforms, with and without a 3-prime iron-responsive element; Dmt1+ire and Dmt1-ire, respectively. To investigate how these isoforms regulate Notch signalling, we stably transduced U9 Notch reporter cells (which only express Dmt1b (Fig. S3A)) with *Dmt1-ire* and *Dmt1+ire* shRNAs (Fig. S3B). Silencing of *Dmt1-ire* reduced Notch reporter activity (Fig. S3C) and *Hey1* and *Hes1* expression (Fig. S3D). Conversely, silencing of the *Dmt1+ire* isoform had the opposite effect, causing increased Notch reporter activity and target gene expression (Fig. S3C,D).

We also used immunostaining and ectopic Dmt1 isoform expression to investigate whether the differences in Dmt1 isoform localization could explain the opposite effects of Dmt1b isoforms on Notch activity (Fig. 4A–C). While *Dmt1b-ire* was expressed in small cytoplasmic speckles and showed (peri-) nuclear accumulation, *Dmt1b+ire* overexpression marked large cytoplasmic speckles (Fig. 4C) that strongly overlapped with the lysosomal marker Lamp1. Together, these data show that different Dmt1 isoforms show different localization, which may be indicative of the different roles in Notch trafficking.

### Dmt1 controls Notch1-mediated cell fate decisions

Because Dmt1 isoforms strongly and oppositely affect Notch signalling, we investigated whether Dmt1 was necessary and sufficient for Notch-mediated cell fate decisions in the Notch-controlled tissues such as muscle, nervous system and intestinal epithelium.

First, we created Dmt1+ire or Dmt1-ire knockdown in murine C2C12 myoblasts. C2C12 cells express both *Dmt1b-ire* and *Dmt1b+ire* isoforms (Fig. S4A). C2C12 cells differentiate into myotubes upon serum starvation, and differentiation is blocked by ectopic Notch1 activation and accelerated by Notch inhibition [28]. When treated with GSI, C2C12 cells displayed accelerated myotube formation (Fig. 5A) with a concomitant increase in myogenic gene expression and downregulation of *Hey1* (Fig. 5B,C). *Dmt1-ire* knockdown (~79%, Fig. 5D) in C2C12 cells resulted in increased myotube formation (Fig. 5A) and premature and increased expression of the muscle differentiation markers, *Msf* (myosin fast) (Fig. 5B), *Myf5*, *MyoD* and *MyoG* (Fig. 5C) [29]. Consistent with the loss of Notch1, *Dmt1-ire* knockdown decreased *Hey1* mRNA after 4 days of C2C12 differentiation (Fig. 4C). In contrast, *Dmt1+ire* knockdown (~76%, Fig. 5D) suppressed myotube formation and muscle cell differentiation, with reduced *MyoD*, *MyoG*, *Myf5* and *Msf* expression (Fig. 5A–C). In line with decreased myoblast differentiation, *Dmt1+ire* knockdown showed enhanced Notch activity through increased *Hey1* expression. The data show that Dmt1 isoform expression is necessary and sufficient to control Notch-mediated muscle cell differentiation in C2C12 cells.

Next, we investigated the role of Dmt1 in Notch-dependent neuronal differentiation [30]. The neuronal differentiation of Neuro2A cells [which only express *Dmt1b* isoforms (Fig. S4B)] is induced by serum depletion and cAMP treatment (Fig. 6A). As expected, GSI treatment enhanced Neuro2A differentiation, as

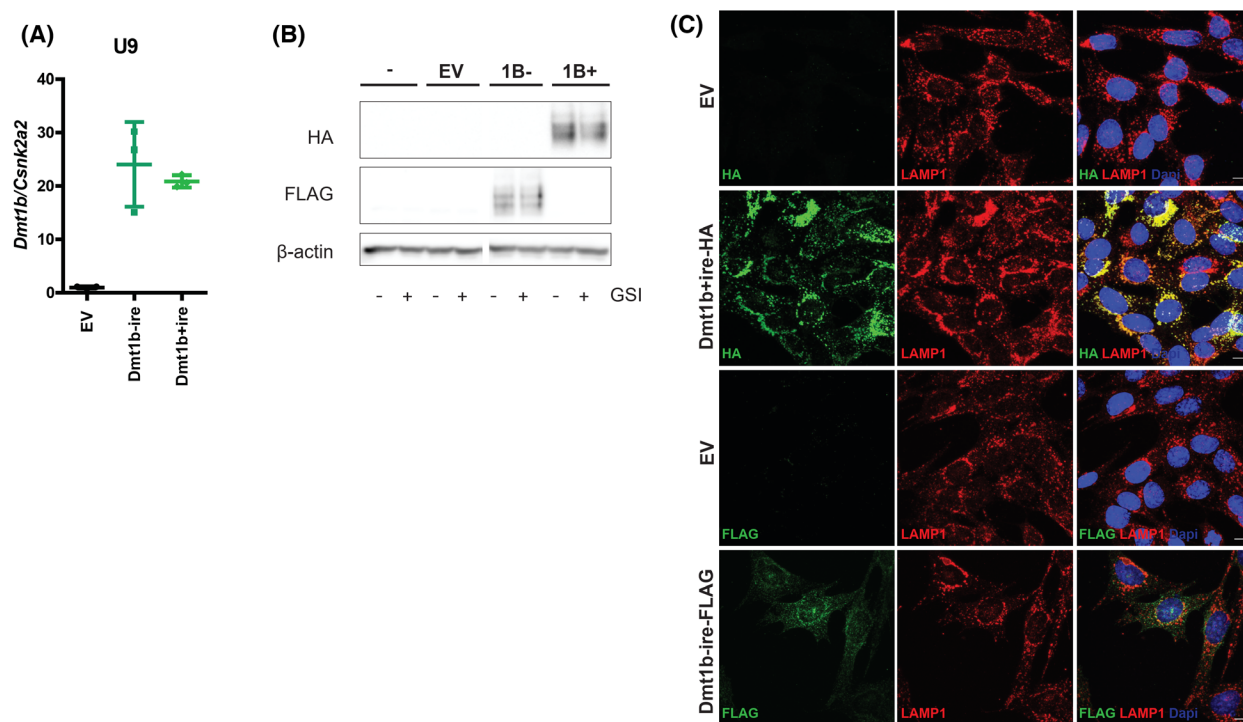


**Fig. 4.** Ectopic expression of Dmt1b+ire localizes to the lysosomes. (A) Dmt1b mRNA expression levels in U9 cells with stable overexpression of empty vector (EV), Dmt1b-ire (1B-) or Dmt1b+ire (1B+). Csnk2a2 mRNA expression was used as a housekeeping control. (B) Immunoblot analysis of HA, FLAG and  $\beta$ -Actin (loading control) protein levels in U9 cells with stable overexpression of empty vector (EV), Dmt1b-ire or Dmt1b+ire treated with DMSO or GSI for 24 h. (C) Immunofluorescence co-staining for HA- or FLAG-tagged Dmt1b isoforms (green) and Lamp1 (red) in U9 cells with stable overexpression of empty vector (EV) or the different Dmt1b isoforms. Cells were counterstained with DAPI. Scale bar: 10  $\mu$ m. GSI,  $\gamma$ -secretase inhibitor dibenzazepine; Lamp1, lysosomal-associated membrane protein 1. Data are representative of three independent experiments, and values are expressed in mean  $\pm$  SD.

measured by the increased number and length of neurites (Fig. 6B,C). Interestingly, under noninducing basal conditions, *Dmt1-ire* knockdown ( $\sim 90\%$ , Fig. 6D) resulted in an increased number of neurites that were further enhanced upon cAMP stimulation and comparable with GSI treatment. Silencing of the *Dmt1+ire* isoforms ( $\sim 65\%$ , Fig. 6D) showed no significant reduction in neuronal differentiation. To test whether the increased neurite formation in *Dmt1-ire* knockdown could be suppressed by ectopic Notch1, we transduced Neuro2A *shDmt1-ire* cells with lentiviral *Nicd1-GFP* (Fig. 7A). *Nicd*-overexpression (GFP+) in *Dmt1-ire* knockdown Neuro2A cells strongly impaired neurite formation (Fig. 7B) and neurite length (Fig. 7C) under both basal and inducing conditions compared with GFP<sup>neg</sup> *shDmt1-ire* Neuro2A cells. These findings demonstrate that constitutive *Nicd1* expression is sufficient for blocking the accelerated neuronal differentiation induced by the loss of *Dmt1-ire* expression and that Dmt1 isoforms function upstream of *Nicd* production.

### Dmt1 isoforms control cell fates in intestinal organoids oppositely

Notch signalling is essential for intestinal cell renewal and differentiation [31–33]. To study Dmt1 function in intestinal homeostasis, we perturbed Dmt1 isoform expression in mouse intestinal organoids using shRNA knockdown. Wild-type intestinal organoids expressing both *Dmt1a* and *Dmt1b* isoforms (Fig. 8A, Fig. S4C) showed a mixed population of immature (sphere-like) and mature (crypt-like) organoids (Fig. 8B). Macroscopically, *Dmt1-ire* knockdown ( $\sim 52\%$ ) resulted in mature crypt-villus-containing mini-guts, while knockdown of *Dmt1+ire* ( $\sim 63\%$ ) resulted in sphere-like organoids (Fig. 8B–D). Moreover, *shDmt1+ire* organoids showed a significantly higher replating capacity than both *shScr* and *shDmt1-ire* knockdown organoids, consistent with their more immature phenotype (Fig. 8E). Typically, both *shScr* and *shDmt1-ire* intestinal organoids displayed columnar organization, microvilli and goblet cells: features lacking in

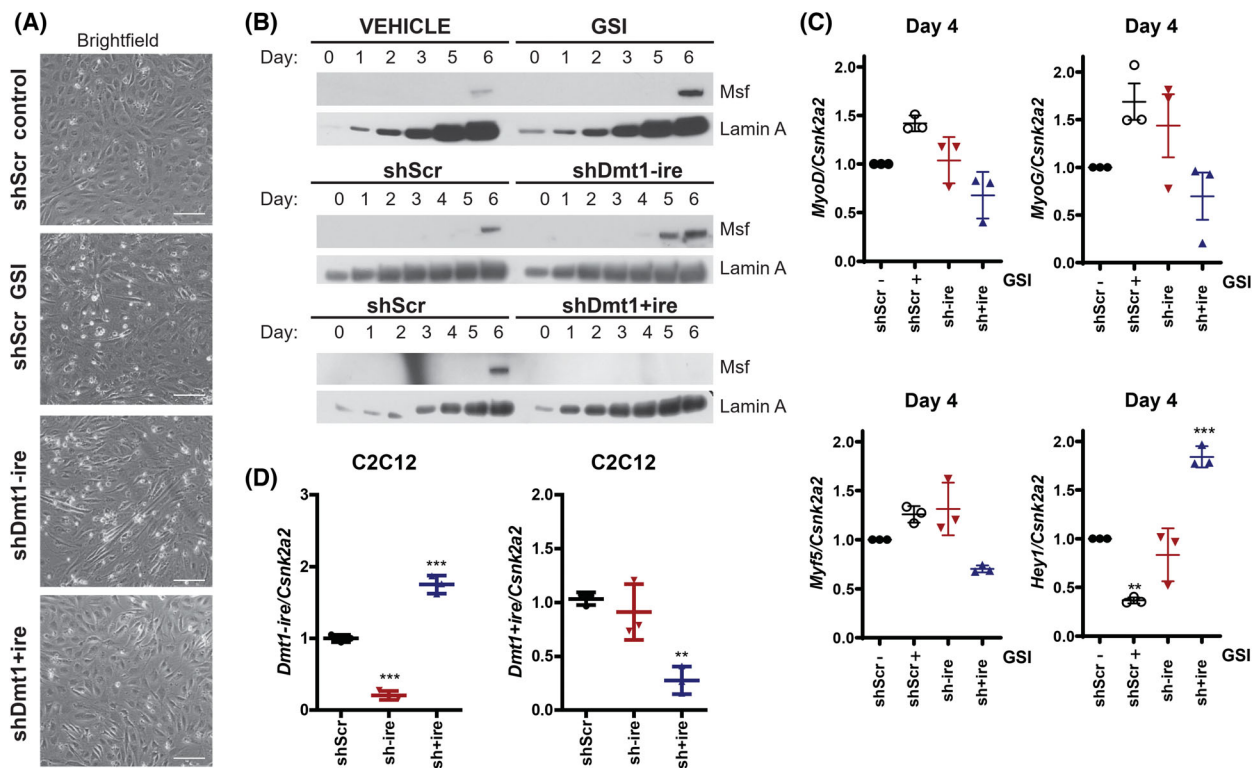


**Fig. 5.** Dmt1 controls Notch1-mediated myoblast differentiation. (A) Bright-field representative images of C2C12 cells differentiated for 6 days. Scale bar: 100 μm. (B) Dmt1-ire and Dmt1+ire mRNA expression in C2C12 cells with stable knockdown of scrambled, Dmt1-ire or Dmt1+ire analysed by qRT-PCR [one-way ANOVA (Tukey comparison),  $**P < 0.01$ ,  $***P < 0.001$ , significantly compared with scrambled control]. Csnk2a2 mRNA expression was used as a housekeeping control. (C) Immunoblot analysis of Msf and lamin A (loading control) protein levels in undifferentiated (Day 0) and differentiated (Days 1–6) C2C12 cells with stable knockdown of scrambled (treated with GSI), Dmt1-ire or Dmt1+ire. (D) qRT-PCR for the mRNA expression of differentiation markers MyoD, MyoG, Myf5 and Notch target gene Hey1 at 4 days postdifferentiation initiation in C2C12 cells with knockdown of scrambled treated with DMSO or GSI, Dmt1-ire or Dmt1+ire. Csnk2a2 mRNA expression was used as a housekeeping control [one-way ANOVA (Tukey comparison),  $**P < 0.01$ ,  $***P < 0.001$ , significantly compared with the DMSO-treated scrambled control]. GSI,  $\gamma$ -secretase-inhibitor dibenzazepine; Msf, myosin skeletal FAST; Myf5, myogenic factor 5; MyoD, myoblast determination protein 1; MyoG, myogenin. Data are representative of three independent experiments, and values are expressed in mean  $\pm$  SD.

*Dmt1+ire* knockdown organoids (Figs 8F and 9A). Silencing of *Dmt1-ire* led to reduced expression of Notch targets, *Hes1* and *c-Myc* (Fig. 9B). In contrast, in immature *Dmt1+ire* knockdown organoids, we observed increased expression of the Wnt/ $\beta$ -catenin stem cell marker, *Asc12* (Fig. 9B) and fetal endodermal stem/progenitor cell genes, *Spp1*, *Trop2* and *Cnx43* (Fig. 9C). These results confirm that isoform-specific loss of Dmt1 results in either the induction (shDmt1-ire) or the suppression (shDmt1+ire) of differentiation through Notch signalling.

### Dmt1 controls Notch activity in human colorectal cancer cells and *Apc*<sup>-/-</sup> organoids

Because Notch deregulation is frequently observed in leukaemia and many solid cancers and the increased

expression of Trop2 is associated with worse outcomes in cancer patients, we examined whether Dmt1 also regulates Notch signalling in human cancer cells. Human colorectal adenocarcinoma (LS174T) cells only express Dmt1b isoforms (Fig. S4D) and retain the ability to differentiate into secretory cells, including goblet cells, upon treatment with GSI [34,35]. In *Dmt1-ire* knockdown (~83%) LS174T cells (Fig. 10A), we observed an increased number of goblet cells (Fig. 10B), elevated *Muc5ac* mRNA (Fig. 10C) and a decrease in the expression of the intestinal stem cell marker *Olfm4* (Fig. 10D) and Notch target genes, *Hes1* and *Hes4* (Fig. 10E). The phenotype of Dmt1-ire LS174T cells strongly resembled those after treatment with GSI. Moreover, immunoblot analysis revealed increased Val1744-cleaved Notch1 upon *Dmt1-ire* silencing (Fig. 10F). We confirmed these findings using

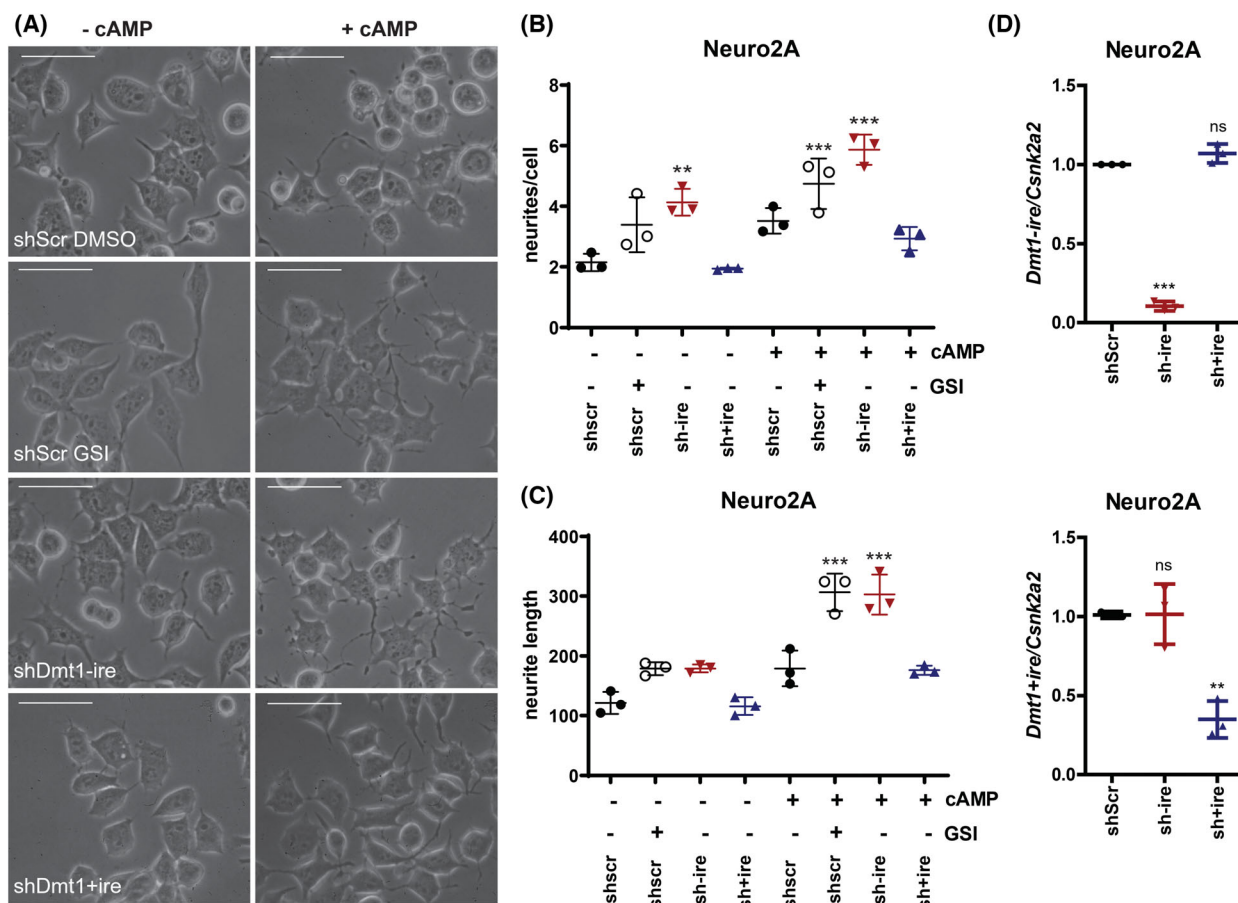


**Fig. 6.** Dmt1 regulates Notch-mediated neuronal differentiation. (A) Bright-field representative images of basal (left, -cAMP) and differentiated (right, +cAMP) Neuro2A cells with knockdown of scrambled (treated with DMSO or GSI), Dmt1-ire, or Dmt1+ire. Scale bar: 50  $\mu$ m. (B, C) Quantification of the number of neurites per cell and neurite length under basal and differentiated conditions (one-way ANOVA [Tukey comparison],  $**P < 0.01$ ,  $***P < 0.001$ , significantly compared with the DMSO-treated scrambled control). (D) Dmt1-ire and Dmt1+ire mRNA expression in Neuro2A cells with stable knockdown of scrambled, Dmt1-ire or Dmt1+ire measured by qRT-PCR. Csnk2a2 mRNA expression was used as a housekeeping control (one-way ANOVA (Tukey comparison), ns, nonsignificant,  $**P < 0.01$ ,  $***P < 0.001$ , significantly compared with scrambled control).

an independent shRNA, targeting a different region of *Dmt1-ire* (#2) (Fig. 10A,E). Taken together, the Dmt1-ire isoform sustains high Notch activity in colorectal cancer cells.

Because most human colorectal cancers have perturbation of the Wnt- $\beta$ -catenin pathway, we utilized murine *Apc*<sup>-/-</sup>-derived intestinal organoids to model colorectal adenoma. *Apc*<sup>-/-</sup> organoids showed a sphere-like phenotype (Fig. 11A), low expression of intestinal differentiation markers (Fig. S5A), and increased *Trop2* and *Hes1* expression (Fig. 11B), analogous to wild-type organoids with knockdown of *Dmt1+ire*. In line with this, both *Dmt1a+ire* and *Dmt1b+ire* expression was diminished in *Apc*<sup>-/-</sup> compared with *Apc*<sup>+/+</sup> intestinal organoids (Fig. 11C). Altogether, decreased *Dmt1+ire* expression in intestinal organoids results in altered intestinal cell fates

by increasing fetal and stem cell identity and blocking epithelial differentiation.

Lastly, we investigated the clinical relevance of Dmt1 isoform expression in a cohort of 113 colorectal peritoneal cancer metastases (RSEM) [36]. We selected two transcripts [ENST00000262052.9\_2 (*Dmt1+ire*) and ENST00000644495.1\_1 (*Dmt1-ire*)] in GENCODE that were expressed throughout the cohort (Fig. S5B). Interestingly, there is no direct correlation between the expression of the two isoforms in this dataset ( $R = 0.093$ ,  $P = 0.328$ , Fig. S5C). When we analysed the ratio of *Dmt1-ire*/*Dmt1+ire* expression, we identified a significant correlation with expression of the Notch target gene *Hes4*. Furthermore, when using *Hes4* as a proxy for Notch activity, the *Dmt1+ire* and *Dmt1-ire* isoform expression in this dataset shows

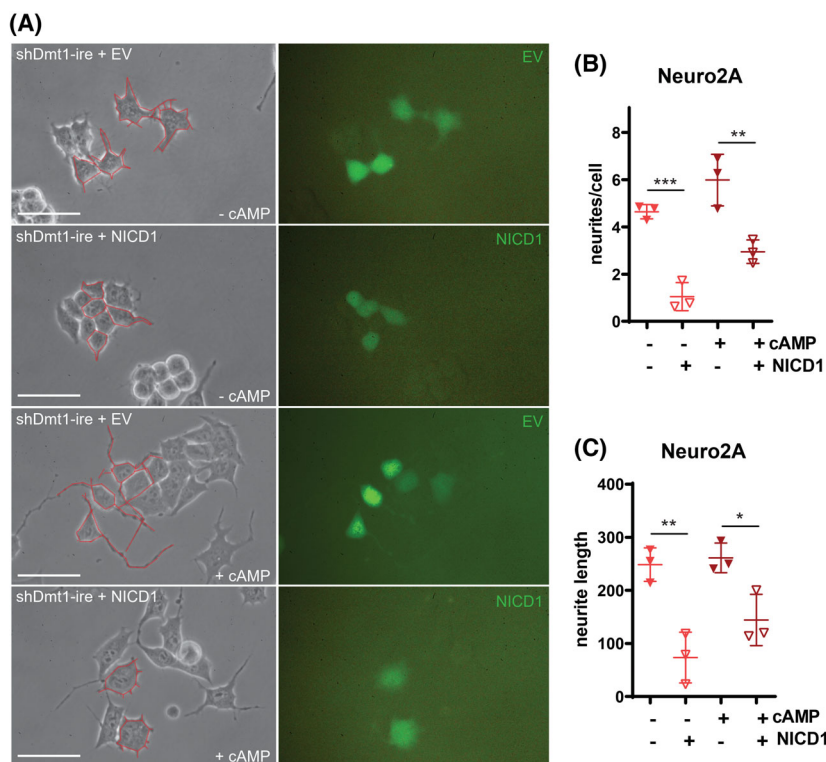


**Fig. 7.** Overexpression of NICD1 rescues shDmt1-ire induced neuronal differentiation. (A) Bright-field and fluorescent images of basal (-cAMP) and differentiated (+cAMP) Neuro2A cells with stable Dmt1-ire knockdown and overexpression of empty vector (GFP) or NICD1 (GFP). GFP-positive cells are outlined in red. Scale bar: 50 μm. Data are representative of three independent experiments, and values are expressed in mean ± SD. (B, C) Quantification of the number of neurites per cell and neurite length in Neuro2A cells with the overexpression of empty vector or Nidc1 and knockdown of Dmt1-ire [one-way ANOVA (Tukey comparison), \* $P < 0.05$ , \*\* $P < 0.01$ , \*\*\* $P < 0.001$ , significantly compared with the control]. GSI,  $\gamma$ -secretase-inhibitor dibenzazepine; Nidc1, Notch1 intracellular domain. Data are representative of three independent experiments, and values are expressed in mean ± SD.

opposite correlations (Fig. 11D). For Dmt1-ire, a significant positive association can be seen only in BRAF mutated CRC ( $R = 0.401$   $P = 0.017$ ). In addition, significant positive correlations were also found for other canonical Notch target genes, including Hey1 and Hey2 with Dmt1 isoform ratio (Dmt1-ire/+ire) (Table S2). Together, these data further support the relevance of distinct Dmt1 isoforms and link its expression to Notch activation in cancer patients.

## Discussion

We identified Dmt1 as an essential novel regulator of Notch signalling and demonstrated that Dmt1 isoforms are opposite regulators of Notch-mediated self-renewal and cell fate. Interestingly, our study highlights the responsiveness of Dmt1 expression to iron, through the presence or absence of the iron response element, as a critical factor in Dmt1 regulation. Therefore, the Dmt1-ire isoform is necessary to sustain Notch signalling, while Dmt1 iron-sensitive isoforms are potent suppressors of Notch activity. Furthermore, the specific modulation of different isoforms leads to opposite effects on Notch-dependent cellular fate in several cell types and in organoid mini-guts where Dmt1 controls the balance between cell renewal and differentiation.

In line with our findings, loss of Apc in colorectal cancer results in the accumulation of iron resulting from increased expression of Tfr1 and Dmt1 through Wnt pathway activation [37]. Furthermore, inhibitors of Dmt1 selectively target cancer stem cells, which are addicted to iron, inducing ferroptosis by blocking lysosomal iron translocation [38]. Finally, Dmt1 is a promising reporter protein for tracking human neural progenitor/stem cells by tracking manganese [39], and iron is essential for human pluripotent stem cells [40]. We observed increased *Trop2* expression in *Dmt1+ire* knockdown organoids and *Apc<sup>-/-</sup>* organoids. The findings are consistent with studies in colorectal cancer showing that *Trop2* expression is associated with high Notch activity, a more malignant phenotype and worse outcomes [41,42]. Thus, our data show an important role for Dmt1 isoforms and iron in stem cell maintenance and demonstrate that these functions involve Notch activity regulation.

Interestingly, we observed high Val1744-cleaved Nidc1 while Notch target genes were decreased in Dmt1 KO MEFs and upon silencing of *Dmt1-ire* in LS174T cells. We previously showed that blocking the vesicular trafficking in cells using chloroquine, or V-ATPase inhibition also led to high levels of Val1744-cleaved Nidc1 in Notch1-mutated T-ALL cells without Notch target gene activation [12]. These findings emphasize that

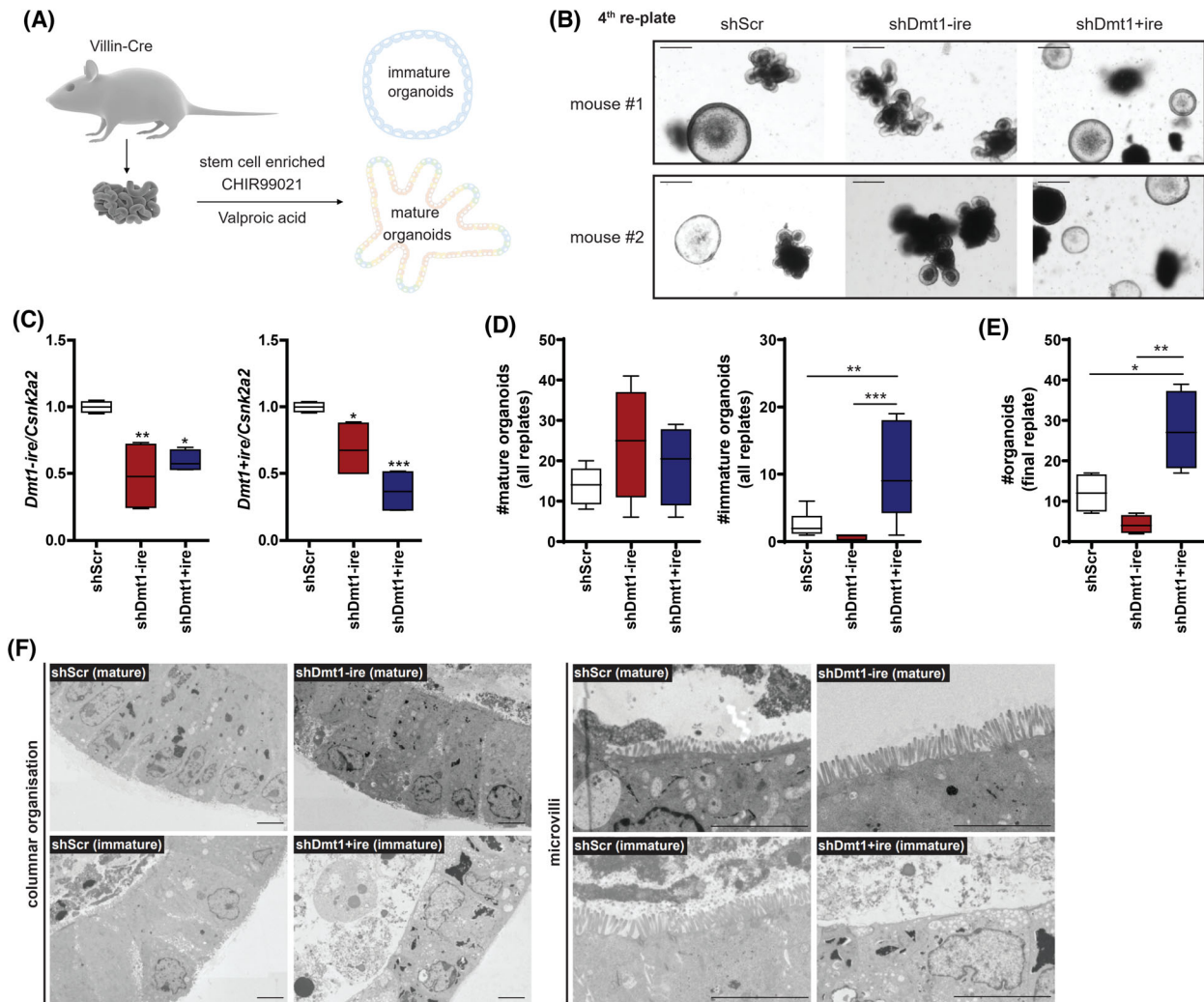
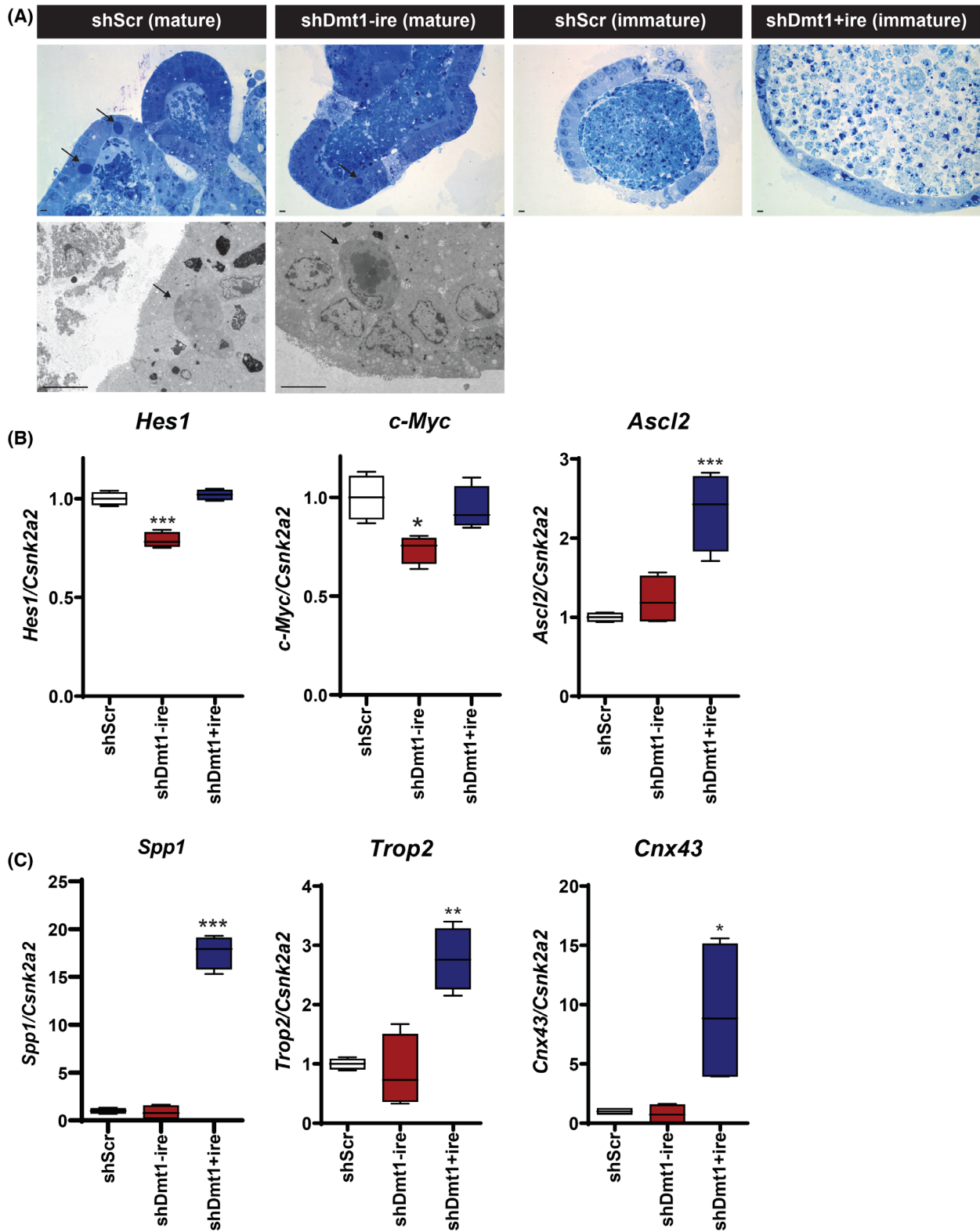


**Fig. 8.** Dmt1 isoforms regulate mouse intestinal organoid differentiation and stemness. (A) Primary mouse intestinal organoids were generated from Villin-Cre mice. A mixed population of immature and mature organoids was obtained after stem cell enrichment. (B) Representative images of mouse intestinal organoids generated after viral transduction with shScrambled (shScr), shDmt1-ire, and shDmt1+ire at the fourth replate. Scale bar: 50  $\mu$ m. (C) Dmt1-ire and Dmt1+ire mRNA expression in mouse intestinal organoids with stable knockdown of Scrambled (Scr), Dmt1-ire or Dmt1+ire analysed by qRT-PCR [one-way ANOVA (Tukey comparison), \*\* $P < 0.01$ , \*\*\* $P < 0.001$ , significantly compared with scrambled control]. Csnk2a2 mRNA expression was used as a housekeeping control. (D) Mature (left) and immature (right) organoid counts in all replates combined from two donor mice [one-way ANOVA (Tukey comparison), \*\* $P < 0.01$ , \*\*\* $P < 0.001$ ]. (E) Total number of organoids in final replate [one-way ANOVA (Tukey comparison), \* $P < 0.05$ , \*\* $P < 0.01$ ]. (F) Representative electron microscopic images of mouse intestinal organoids transduced with hairpins against Scr, Dmt1-ire and Dmt1+ire. shScr (mature and immature) and shDmt1-ire organoids showed columnar organization (top panel) and well-established microvilli (bottom panel), both of which were lost in shDmt1+ire organoids. Scale bar: 5  $\mu$ m. The experiment was performed using intestinal stem cells obtained from two individual donor mice, and values are expressed in mean  $\pm$  SD.

Val1744-Notch1 cleavage is not sufficient for Notch1 activity and that subsequent intracellular events are rate limiting [12,43]. Since *Nicd1* rescues the phenotype of Dmt1 KO MEFs, Dmt1 acts upstream or parallel to the NICD/RBP-jk transcriptional regulation. Therefore, our work demonstrates that  $\gamma$ -secretase cleavage and Val1744-*Nicd1* expression are insufficient for Notch1

transcriptional activity and caution against the use of Val1744 as a single biomarker for Notch1 activity. While ectopic *Nicd1* expression rescued the Notch signalling defects in Dmt1 KO and Neuro2A shDmt1-ire, overexpression of a Notch1 gain-of-function T-ALL mutant in *Adam10*<sup>-/-</sup>17<sup>-/-</sup> deficient cells was not sufficient to restore Notch activity upon *Dmt1-ire* silencing.



This observation is consistent with the identification of the shRNA targeting the *Dmt1-ire* isoform in our screen. Consistent with the increase in Notch1 surface

expression upon loss of Dmt1, we propose that Dmt1 function involves Notch regulation in vesicles and trafficking.

**Fig. 9.** Dmt1 isoforms regulate Notch signalling and fetal transcript programs in mouse intestinal organoids. (A) Toluidine blue and electron microscopy was used to detect goblet cells (black arrows) in primary mouse intestinal organoids with stable knockdown of Scr, Dmt1-ire or Dmt1+ire. Scale bar: 5  $\mu$ m. The experiment was performed using stem cells derived from two individual donor mice, unless stated otherwise, and values are expressed in mean  $\pm$  SD. (B) mRNA expression levels of Notch target genes, Hes1 and c-Myc, and Wnt target gene Ascl2 in shScr, shDmt1-ire and shDmt1+ire mouse intestinal organoids measured by qRT-PCR. Csnk2a2 mRNA expression was used as a housekeeping control [one-way ANOVA (Tukey comparison), \* $P$  < 0.05, \*\*\* $P$  < 0.001, significantly compared with shScr organoids]. (C) Fetal transcript program genes Spp1, Trop2 and Cnx43 mRNA expression in shScr, shDmt1-ire and shDmt1+ire mouse intestinal organoids, measured by qRT-PCR. Csnk2a2 mRNA expression was employed as a housekeeping control [one-way ANOVA (Tukey comparison), \* $P$  < 0.05, \*\* $P$  < 0.01, \*\*\* $P$  < 0.001, significantly compared with shScr organoids]. The experiment was performed using intestinal stem cells obtained from two individual donor mice, and values are expressed in mean  $\pm$  SD.

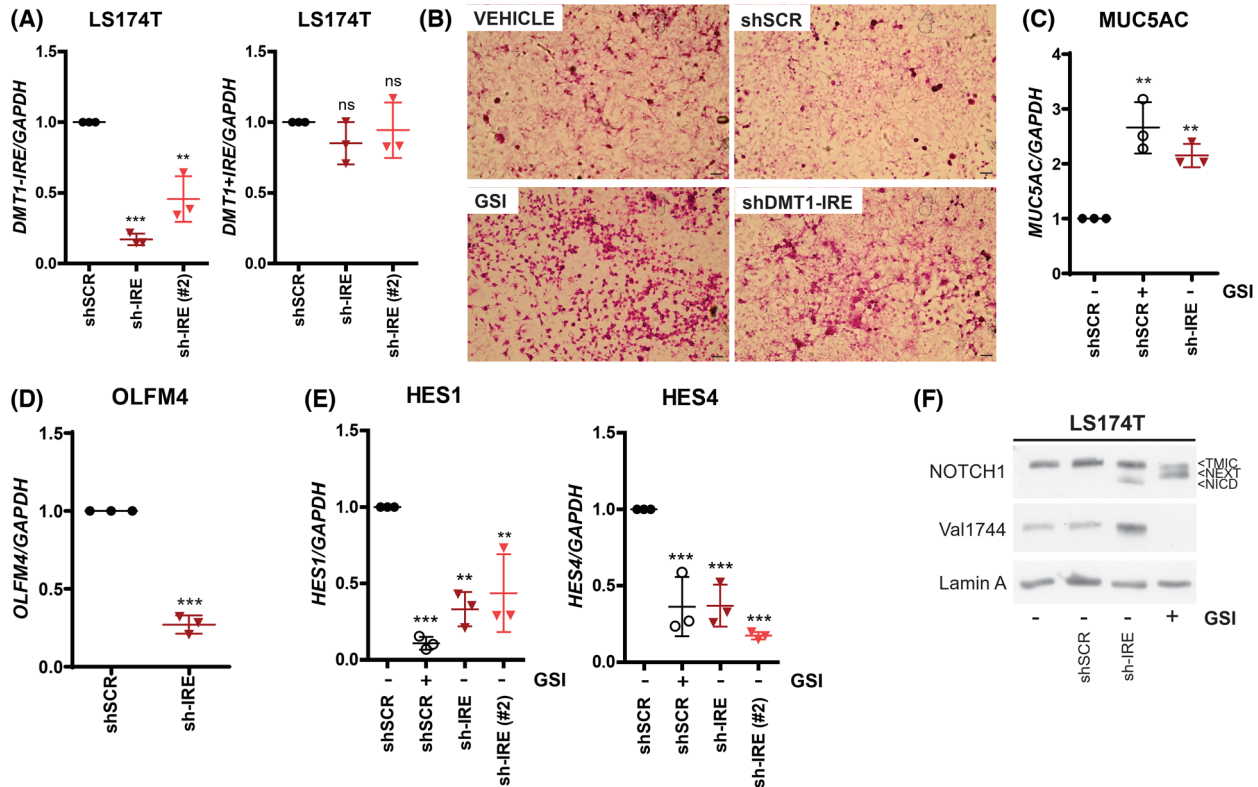


**Fig. 10.** Dmt1 regulates Notch signalling and differentiation in human colorectal cancer cells. (A) qRT-PCR for Dmt1-IRE and Dmt1+IRE mRNA expression in LS174T cells with stable knockdown of scrambled (shSCR) or Dmt1-IRE (sh-IRE) [one-way ANOVA (Tukey comparison), ns, nonsignificant, \*\* $P$  < 0.01, \*\*\* $P$  < 0.001, significantly compared with scrambled control]. An independent hairpin targeting another sequence of Dmt1-IRE was used as a control (sh-IRE#2). GAPDH mRNA expression was used as a housekeeping control. (B) Periodic Acid–Schiff (PAS) staining in LS174T cells treated with DMSO or GSI for 7 days or LS174T cells with stable knockdown of SCRAMBLED (SCR) or Dmt1-ire. Scale bar: 50  $\mu$ m. (C) qRT-PCR for mRNA levels of MUC5AC in shSCR cells treated with DMSO or GSI for 7 days and shDmt1-IRE cells. GAPDH was used as a housekeeping control [one-way ANOVA (Tukey comparison), \*\* $P$  < 0.01, significantly compared with the DMSO control]. (D) OLFM4 mRNA expression in LS174T cells with knockdown of Dmt1-IRE, measured by qRT-PCR. GAPDH was employed as a housekeeping control (Student *t*-test, \*\*\* $P$  < 0.001, significantly compared with the scrambled control). (E) qRT-PCR for Notch target gene (HES1, HES4) mRNA expression in LS174T cells with knockdown of SCR (treated with DMSO or GSI for 7 days) or Dmt1-IRE (and independent hairpin sh-IRE #2). GAPDH was used as a housekeeping control [one-way ANOVA (Tukey comparison), \*\*\* $P$  < 0.01, \*\*\* $P$  < 0.001, significantly compared with the scrambled control]. (F) Immunoblot analysis of protein levels of Notch1 (C-20), Val1744 and lamin A (loading control) in LS174T cells with knockdown of SCR (treated with DMSO or GSI for 7 days) or Dmt1-IRE. GSI,  $\gamma$ -secretase inhibitor dibenzazepine; NEXT, Notch1 extracellular truncation; TMIC, transmembrane/intracellular fragment. Data are representative of three independent experiments, and values are expressed in mean  $\pm$  SD.

Dmt1 loss disrupted vesicular trafficking, increased endocytosis, increased expression of endo- and lysosomal markers, and increased basal autophagic flux. In

Eeal-positive endosomes, surface proteins are transported directly from the cell surface to the nucleus [44]. The increased levels of Eeal upon loss of Dmt1

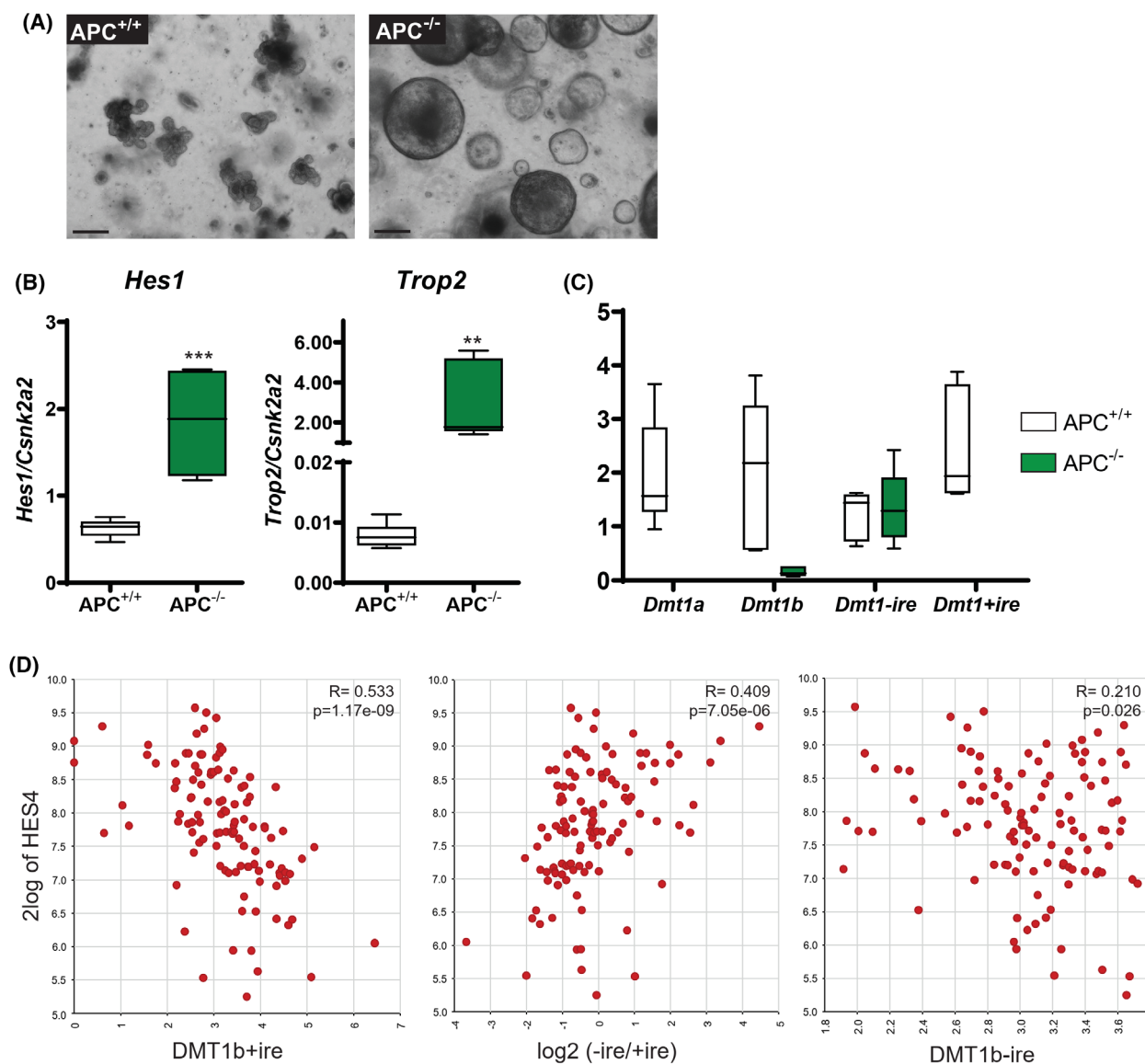


**Fig. 11.** Dmt1 isoform expression correlates with Notch target gene expression in peritoneal CRC metastases. (A) Representative bright-field images of *APC*<sup>+/+</sup> and *APC*<sup>-/-</sup> mouse intestinal organoids. Scale bar: 50  $\mu$ m. (B) *Hes1* and *Trop2* mRNA expression in *APC*<sup>+/+</sup> and *APC*<sup>-/-</sup> mouse intestinal organoids, measured by qRT-PCR. *Csnk2a2* mRNA expression was utilized as a housekeeping control (Student *t*-test, \*\* $P < 0.01$ , \*\*\* $P < 0.001$ , significantly compared with *APC*<sup>+/+</sup> organoids). (C) qRT-PCR for mRNA levels of *Dmt1* isoforms in *Apc*<sup>+/+</sup> and *Apc*<sup>-/-</sup> intestinal organoids. *Csnk2a2* mRNA expression was utilized as a housekeeping control. (D) Correlations between *Dmt1+ire* ( $R = -0.533$ ,  $P = 1.17e-09$ ), the ratio of *Dmt1-ire/+ire* ( $R = 0.409$ ,  $P = 7.05e-06$ ) and *Dmt1-ire* ( $R = 0.210$ ,  $P = 0.026$ ), and HES4 (Notch target gene) expression (log<sub>2</sub>) in tumour colon metastases [cohort of 113 colorectal peritoneal cancer metastases (RSEM)]. Data are representative of three independent experiments, and intestinal stem cells were derived from three individual donor mice per condition (*Apc*<sup>-/-</sup> and *Apc*<sup>+/+</sup>). Values are expressed in mean  $\pm$  SD.

may disrupt full-length and S2-cleaved Notch transport and activation. In addition, loss of *Dmt1* resulted in damaged intracellular vesicles with disrupted/missing membranes and the formation of isolation membranes, which is characteristic of the formation of phagophores, an early step in autophagy/lysophagy [45]. Lysosomal membrane damage may occur in

*Dmt1* KO MEFs due to the accumulation and disbalance of cytoplasmic and vesicular iron, causing oxidative stress that results in lysosomal membrane peroxidation [46]. Lysosomal damage is sensed by cathepsins which trigger lysophagy, the selective autophagy of lysosomes, which correlates with the elevated basal autophagy flux in *Dmt1* KO MEFs [45]. These

findings support observations that blocking vesicle function inhibits Notch-dependent T-ALL growth and leads to ROS accumulation [12]. Consistently, chloroquine was less effective in raising the intravesicular pH in Dmt1 KO MEFs, reflecting perturbed trafficking and a lysosome defect. The  $\gamma$ -secretase complex, which is present on the plasma membrane, endocytic compartments and lysosomes [11,47], shows more efficient S3-cleavage in endocytic compartments, which have a lower pH [8,48]. Together with the finding that defects in vATP-ase reduce Notch signalling [49], these data support the notion that perturbations in vesicular trafficking and pH caused by loss of Dmt1 result in an accumulation of inactive Notch/Nicd in vesicles.

Previous studies have shown that intracellular ROS levels regulate Notch signalling in airway basal stem cells through Nrf2-dependent Notch signalling [50]. These observations raise the possibility that ROS levels can directly inactivate the Notch pathway by reducing NICD degradation that could contribute to observed phenotypes. Further experiments will be needed to dissect the direct and indirect roles of ROS on the Notch pathway.

In this study, we report that Dmt1-ire loss phenocopies Notch is a loss of function phenotype in muscle, neurons, intestinal organoids and human cancer tissues. However, Dmt1 knockout mice are viable while Notch1 knockouts are embryonic lethal. This suggests that Dmt1 is not important for all tissues that require Notch signalling. Another explanation could be that Dmt1 knockouts do not express any Dmt1 isoform. Dmt1-ire specific isoform knockout mice (retaining Dmt1+ire expression) could address this question. Our findings warrant further investigation into the regulation of Notch activity by Dmt1 in specific tissues.

Others have also shown that *Dmt1-ire* is expressed in early, sorting and recycling endosomes [51–53]. Our study highlighted that *Dmt1b-ire* is expressed in intracellular vesicles with minor co-localization to lysosomes, while *Dmt1b+ire* is almost exclusively located in the lysosomes. Therefore, we speculate that *Dmt1b-ire* promotes Notch intracellular trafficking and receptor processing in early, sorting and recycling endosomes to promote Notch activity [54], whereas *Dmt1+ire* isoform promotes lysosomal degradation to turn off Notch activity. If and how iron is controlling Dmt1 isoform localization, expression and activity requires further study.

A relation between iron and Notch signalling has been reported before. For example, iron drives the proliferation of Notch-induced T-ALL in mice [55] and breast cancer cells upregulate Dmt1 to import iron [56]. Beyond iron, Dmt1 transports other divalent metals, including  $\text{Zn}^{2+}$ ,  $\text{Co}^{2+}$ ,  $\text{Cu}^{2+}$  and  $\text{Mn}^{2+}$  [57]. Importantly, zinc is required for Notch-S2 shedding

by Adam10 [7,58] and  $\gamma$ -secretase activity is modulated by zinc and copper [59]. Further research is needed to establish if and how Notch activity and iron/divalent metal signalling are hardwired.

The ubiquitous expression of Dmt1b in many tissues during development and in adult tissues [22] may suggest a general role of Dmt1 in regulating stem cell renewal and cell fate. Our study primarily focused on the role of Dmt1 on Notch1 activity. Mammalian cells encode for four Notch receptors, and whether Dmt1 isoforms also control these remains unknown. Further research is needed to identify how Dmt1 isoform expression and iron transport are regulated in tissues and their relation to Notch transcriptional activity. Although we provide evidence for the critical role played by Dmt1 isoforms in Notch activation cascade, the precise identity of the vesicles through which Dmt1 regulates Notch cell fates requires further study.

Finally, we show that Dmt1 isoform expression in colorectal cancers may have clinical relevance and implication and correlate with expression of canonical Notch target genes. It has been previously shown that tumour expression of DMT1 is elevated in CRC patients [60]; however, Dmt1 isoform expression is not assessed. Therefore, further validation in different CRC clinical subtypes is necessary but the role of Notch in CRC is supported by literature and the *in vitro* models presented here. Together, these findings warrant a further investigation into the role of Dmt1 as a biomarker and therapeutic target in cancer. In addition, our data imply that pharmacological inhibition of *Dmt1-ire* isoforms may be employed to curtail Notch signalling in cancers. At the same time, *Dmt1+ire* inhibitors might augment Notch signalling to specify cell fates or promote tissue regeneration.

To conclude, we identified Dmt1 as a novel regulator of Notch activity, which, in an isoform-specific manner, determines the fate of the Notch signalling cascade between  $\gamma$ -secretase cleavage and downstream transcriptional activation. Furthermore, our data demonstrate that the current paradigm of  $\gamma$ -secretase cleavage equating Notch activation is incomplete. We propose that Dmt1-containing intracellular vesicles represent a new and essential rate-limiting step through which Notch receptors traverse to control cell fate in normal tissues and diseases.

## Materials and methods

### Compounds

Cells were treated with dimethyl sulfoxide (DMSO), 0.2  $\mu\text{M}$  of  $\gamma$ -secretase inhibitor dibenzazepine (DBZ) (Syncom,

Groningen, The Netherlands) dissolved in DMSO, 30  $\mu\text{M}$  of 2-(3-carbamimidoyl-sulfanylmethyl-benzyl)-Isothiourea (CISMBI) dissolved in DMSO (Merck, cat. #s302678) or 1  $\mu\text{g}\cdot\text{mL}^{-1}$  of Doxycycline (Sigma, cat. #D9891) dissolved in water, as indicated, unless stated otherwise. Neuro2A cells were stimulated with 0.3 mM of dibutyl-cAMP (Bio Connect, cat. #sc-201567A) dissolved in DMSO. Chloroquine diphosphate salt (Sigma Aldrich) and Bafilomycin A1 (Sigma) were dissolved in deionized water, and cells were treated with 15  $\mu\text{M}$  of chloroquine or 1 nM of Bafilomycin A1 for 24 h.

### shRNA constructs

The pLKO.1-TRC cloning vector, a gift from David Root (Addgene, cat. #10878) [61], was used to generate our different shRNA constructs according to Addgene's pLKO.1 protocol. Primers: pLKOHygroF: 5'-CGGGATCCGCCG CCACCATGCCTGAACTCAC CGCGACGTCTG-3' and pLKOHygroR: 5'-CGGGTACCGCTATTCCTTTGCC TCGGACG-3' were used to PCR amplify the hygromycin gene from a pcDNA5FRT vector used as a template in order to replace the puromycin gene from our pLKO.1-puro vector with the hygromycin resistance gene using the BamHI-KpnI restriction sites in the TRC cloning (stuffer) vector. Functional hairpins were sub-cloned from their puromycin to the hygromycin vector with either a BbvCI-BamHI digest to swap the hairpins or a BamHI-KpnI digest to swap the resistance cassettes in the backbones. The pLKO.1 vector scramble shRNA was a gift from David Sabatini (Addgene, cat. #1864) [62]. Enzymes used were purchased from New England BioLabs, Ipswich, MA, USA. All vectors used were verified by sequencing. Targeting sequences are listed in Table S3.

### Viral vectors

pGL4.24 12xCSL Luc2P-[minP] [5] was digested with NheI-EcoRV, and a fragment was isolated and ligated into a SpeI digested pGreenFire1 vector (SBI) that was blunted with Klenow (in addition of dNTPs) sequentially digested with XbaI, purified from a gel and CIP treated. This resulted in the lentiviral Notch reporter plasmid 12xCSL-GFP-Luc. pBABE-Notch1-L1594-6xMyc was generated by ligating an BamHI-HincII fragment with a BamHI-XbaI (blunted) fragment into pCS2- $\Delta$ EGF-Notch1-L1594P-6xMyc [7]. pBABE-puro JAGGED2-3xMYC as described previously [5].

pCW57-MCS1-P2A-MCS2 (Blast) was a gift from Adam Karpf (Addgene, cat. #80921) [63]. In this lentiviral vector, the Notch1 $\Delta$ E-RFP cDNA was sub-cloned in the NheI site of this vector. The cDNA was retrieved with an SpeI and XbaI digest from a construct, recently published by our laboratory [12], to express an inducible Notch1 $\Delta$ E-RFP (Tet-On). In this backbone, the N terminus was replaced by ligation with a PmeI-BclI fragment,

from an unpublished vector pcDNA/FRT/TO-3xFLAG-mNidc, that we generated using the 3XFlagNidc plasmid a gift from Raphael Kopan (Addgene, cat. #20183) [64], after digestion with SrfI-BclI, generating a lentiviral vector 3xFLAG-Nidc1-RFP (Tet-On). These two backbone vectors were used to replace the RFP at the C terminus with a MluI flanked gBlock encoding a fusion of mCherry with GFP based on the vector sequence of pBABE-puro mCherry-EGFP-LC3B (Addgene, cat. #22418) after digestion with MluI, generating lentiviral vectors Notch1 $\Delta$ E-mCherry-GFP (Tet-On) and 3xFLAG-Nidc1-mCherry-GFP (Tet-On), respectively. Lentiviral vector FUCGW-hNidc-FLAG was a kind gift of David Spencer [65]. This vector was digested with EcoRI removing hNidc-FLAG and back ligated to generate the FUCGW empty vector.

The pDEST30-mDmt1bnonire FLAG vector was a kind gift from Michael Garrick [66]. The cDNA including the 5'prime UTR was retrieved from this vector by an EcoRV digest, and the fragment was sub-cloned in the mung bean blunted, sequentially CIP treated, and PacI site digested into the retroviral pQCXIH vector. In order to generate the +ire isoforms of Dmt1, a gBlock encoding from the BclI site, the N-terminal sequence of these cDNAs followed by an MluI flanked HA-tag, stop-codon and flanking XhoI site was generated and sub-cloned in the pQCXIH and pQCXIN by use of the XhoI and ApaI sites in these vectors. The plasmid's digested and CIP-treated MluI site was used to replace the HA-tag by FLAG annealing and ligating with phosphorylated oligo's MLUflagPMEsense: 5'-CGCGTGTAACTCACTTGTCGTCATCGTCTTT GTAGT CAGTA-3' and MLUflagPME-sense: 5'-CGCG TACTGACTACAAAGACGATGAC GACAAGTGAGT-TTAAACA-3' containing a unique PmeI site for analysis of the isolated plasmids. This resulted in generation of all four C-terminal tagged Dmt1 isoform encoding cDNAs in different selectable retroviral vectors: pQCXIH-Dmt1b-ire-FLAG and pQCXIH-Dmt1b+ire-HA. Enzymes used were purchased from New England BioLabs. All vectors used were verified by sequencing. Lentiviral packaging vectors were derived from the Trono [67] and Weinberg [68] laboratories, and pseudo- or lentiviral production was described previously [5].

### Generation of the Notch reporter (screening) cell line

Adam10<sup>-/-</sup>17<sup>-/-</sup> MEFs [5], devoid of physiological ligand-dependent Notch signalling, were transduced with a 12xCSL-GFP-Luc reporter and  $\Delta$ EGF-Notch1-L1594P-6xMYC vector with a puromycin selectable. First, monoclonal cell lines were generated by single-cell seeding and selecting GFP-positive clones (an indication for Notch activity) for expansion. Next, a clone was selected that showed high luciferase counts, which were significantly

inhibited after  $\gamma$ -secretase inhibition (GSI) (Fig. S1A,B) and is referred to as screening cell line (U9).

### Genetic screen

Lentiviral shRNA libraries were kindly provided and developed by Collecta (Mountain View, CA, USA) based on NIH-funded research grant support 44RR024095 and 44HG003355. We screened the Collecta DECIPHER shRNA Library Disease-Associated Targets (Mouse Module 2) against 4520 Targets containing 27 500 hairpins in the pRSII2 vector, expressing TagRFP (Collecta, cat. #DMDAC-M2V2-P). A transfection mix of 120  $\mu$ g of Module 2 plasmid DNA, 120  $\mu$ g of psPAX2 (a gift from Didier Trono) (Addgene, cat. #12260) and 120  $\mu$ g of pCMV-VSV-G (a gift from Bob Weinberg) (Addgene, #8454) [68] plasmids in DMEM (Dulbecco's Modified Eagle's medium, Sigma) without additives was prepared. Poly(ethylenimine) (P-PEI, 25 kDa, pH 5.0) was added, and the transfection mix was incubated for 15 min at the room temperature. The transfection mix (38  $\mu$ g of plasmid mix) was applied to sub-confluent 293FT cells and incubated for 24 h at 37 °C. After 24 h, cells showed red fluorescence, and the medium was replaced. At 48 h post-transfection, the virus-containing medium was harvested through a 0.45- $\mu$ m filter. The presence of the virus was checked by using a GoStick (Takara Bio Europe) and was found positive. Cells from our screening cell line were transduced in the presence of polybrene (1  $\mu$ g·mL<sup>-1</sup>) at an MOI of 0.7, in which 50% of the cells should become TagRFP positive with one hairpin per cell. At 48 h post-infection, TagRFP expression showed that 51.5% of the transduced cells were RFP positive.

### Distribution and pathway analysis

The average count of reads per gene was calculated in each independent screen run. The distribution of the average of two independent screen runs per gene was generated, and the cumulative frequency distribution of the reads was generated. Screen hits were defined as those in the top 5% of the distribution of the cumulative reads (cut-off: average reads = 2800). GSEA analysis (GO\_Molecular\_Function dataset) was performed using ToppFun on the screen hits.

### Generation of Dmt1 KO MEFs

mNramp2(Dmt1) fl/fl MEFs were a kind gift from Sara Cherry. For genetic typing, primer combinations F1-R1 and F1-R9 were used as described previously [69]. Dmt1 KO clones were generated by transduction with Adeno-Cre or Adeno-dsRED as a control (5.0  $\times$  10<sup>12</sup> particles·mL<sup>-1</sup>, 1 : 1000, VDR). The medium was replaced at 48 h post-transduction. Three days

post-transduction, single-cell suspensions were generated and expanded to obtain single-cell-derived clones.

### Cell lines

Screening cell line (U9) MEFs (Adam10<sup>-/-</sup>17<sup>-/-</sup> MEFs,  $\Delta$ -EGF-Notch1-L1594P-6xMYC, 12xCSL-GFP-Luc), mNramp2fl/fl MEFs, Neuro2A cells (a kind gift from Pilar Martinez-Martinez), LS174T cells (a kind gift from Marc van de Wetering) and U2OS/JAGGED2 cells [70] were maintained in DMEM (Dulbecco's Modified Eagle's medium; Sigma) containing 10% FBS and 50 U·mL<sup>-1</sup> of Penicillin/Streptomycin. In addition, C2C12 cells (a kind gift from Ramon Langen) were maintained in DMEM (Dulbecco's Modified Eagle's medium, high glucose; Gibco) containing 10% FBS and 50 U·mL<sup>-1</sup> of Penicillin/Streptomycin (growth medium). All cell lines were maintained under cell culture conditions (37 °C, 5% CO<sub>2</sub>) and regularly tested for mycoplasma contamination.

### Calcein quenching assay

Dmt1 transport activity was detected as described previously [71]. In short, Dmt1 transport activity was measured by loading cells with 0.25  $\mu$ M of calcein-AM (Invitrogen, Thermofisher, Waltham, MA, USA; cat. # C3100MP) for 20 min at 37 °C in DMEM supplemented with 20 mM of HEPES. Cells were washed with 1XPBS and resuspended in transport buffer (150 mM NaCl, 20 mM of MES, pH 6.0). Fluorescence (excitation 485 nm, emission 520 nm) was recorded using a FLUOstar Omega multi-mode microplate reader (BMG Labtech, Ortenberg, Germany). Baseline fluorescence was measured for 20 s (every 2 s), 100  $\mu$ M of CoCl<sub>2</sub> or Ammonium iron (II) sulfate hexahydrate (FAS, Sigma, cat. #F2262) was added to the cells, and quenching of fluorescence was measured every 0.5 s for 150 s. Fluorescent counts were corrected for baseline fluorescence.

### Notch activity reporter assay

Cells were seeded and treated for 24 h with DMSO, 800 nM of DBZ, 15  $\mu$ M of chloroquine or 1 nM of Bafilomycin A1. After 24 h, luciferase activity was measured using a dual-luciferase reporter assay system (Promega, Madison WI, USA; cat. #E1910) according to the manufacturer's protocol or GFP fluorescence was measured by flow cytometry using a FACSCantoII cytometer with BD FACSDIVA 6.1.1 software, Becton Dickinson (BD), Franklin Lakes, NY, USA. Cells were lysed in 1XPassive Lysis Buffer for luciferase measurements and incubated for 20 min on a shaker at room temperature. Luciferase activity was measured in cell lysates by adding a 1:1 firefly luciferin substrate using a FLUOstar Omega multi-mode microplate reader (BMG Labtech).

## Notch stimulation by ligand

Delta-like 4 (Dll4) stimulation was performed using recombinant human Dll4 (R&D Systems, Minneapolis, MN, USA; cat. #1506-D4-050/CF). Plates were coated with  $5 \mu\text{g}\cdot\text{mL}^{-1}$  of Dll4 in 0.2% gelatin 0.1% BSA in 1XPBS for 24 h at 4 °C. Control well plates were coated with 0.2% gelatin 0.1% BSA in 1XPBS. Cells were seeded on coated plates and incubated for 24 h at 37 °C. JAGGED2 stimulation was performed by seeding U2OS cells constitutively expressing JAGGED2 in 6-well plates. U2OS cells were used as a control. After 24 h, cells were fixed in 4% PFA in 1XPBS for 15 min at room temperature. U2OS cells were washed with 1XPBS and added on top for 24 h at 37 °C for ligand stimulation. Dmt1 wild-type (WT) and knockout (KO) MEFs stably expressing JAGGED2-3xMYC were seeded sub-confluent treated with DMSO or DBZ for 24 h at 37 °C. After 24 h, Dmt1 WT or KO MEFs stably expressing JAGGED2-3xMyc were seeded on top, treated with DMSO or DBZ and incubated for another 24 h to ensure Notch activation by ligand binding.

## Transferrin and dextran uptake assay

Cells were serum-starved for 30 min at 37 °C. After serum starvation, cells were incubated with  $10 \mu\text{g}\cdot\text{mL}^{-1}$  of mouse FITC-labelled transferrin (Jackson ImmunoResearch, Cambridgeshire, UK; cat. #015-090-050) for 10 min at 37 °C, or  $40 \mu\text{g}\cdot\text{mL}^{-1}$  of Alexa488-labelled dextran (Thermo Fisher Scientific, Waltham, MA, USA, cat. #D22910) for 60 min at 37 °C, or  $0.5 \text{mg}\cdot\text{mL}^{-1}$  LysoSensor yellow/blue dextran (Thermo Fisher Scientific, cat. #L22460) for 24 h at 37 °C. For a pulse-and-chase assay, FITC transferrin was removed after a pulse of 10 min, washed with 1XPBS and chased for 50 min at 37 °C. Cells were washed with 1XPBS, trypsinized and analysed by flow cytometry using a FACSCantoII cytometer with BD BD FACSDIV 6.1.1 software. Mean fluorescent intensity (MFI) was determined, corrected for background and normalized to the control to obtain the fold change in transferrin or dextran fluorescence.

## C2C12 differentiation

C2C12 cells were grown at medium passage number (10–20) and maintained in the growth medium. Myogenic differentiation was induced according to a previously published protocol [72]. In short, Matrigel (Corning, cat. #356230) was diluted 1 : 50 in DMEM (high glucose) without any additives and incubated for 30 min at 37 °C to coat the wells or coverslips for C2C12 differentiation. After 30 min, the Matrigel dilution was removed, and cells in the growth medium were added on top of the Matrigel coating and were treated with DMSO or 800 nM of DBZ. After 24 h, cells were washed with 1XPBS, and differentiation medium (DMEM, high glucose, Gibco, ThermoFisher,

Waltham, MA, USA, containing 0.5% heat-inactivated FBS and  $50 \text{U}\cdot\text{mL}^{-1}$  of Penicillin/Streptomycin) was added. Undifferentiated and differentiated cells up to 6 days postdifferentiation initiation were analysed for myotube formation and expression of differentiation markers.

## Neuro2A differentiation

Neuro2A cells were passed through a cell strainer and sparsely seeded in DMEM containing 10% FBS and  $50 \text{U}\cdot\text{mL}^{-1}$  of Penicillin/Streptomycin, and treatments with DMSO or 800 nM of DBZ were added. After 24 h, pictures were taken from undifferentiated Neuro2A cells, washed with 1XPBS, and DMEM without any additives containing 0.3 mM of dibutyryl-cAMP (Bio Connect, cat. #sc-201567A) was added to the cells for 4 h at 37 °C. After 4 h, pictures were taken from differentiated Neuro2A cells, and differentiation was analysed by counting the neurites/cell and neurite length using ImageJ.

## Immunofluorescence

For *Lamp1* staining in U9 cells with Dmt1 isoform overexpression, cells were fixed in methanol for 15 min at  $-20 \text{ }^{\circ}\text{C}$ . Next, cells were washed with 1XPBS, blocked and permeabilized in 5% NGS 0.2% Triton X 1% BSA in 1XPBS (blocking solution) for 30 min at room temperature. After blocking, cells were incubated with rat anti-Lamp1 (1 : 200, Abcam, Cambridge, UK; cat. #ab24170) in blocking solution at 4 °C overnight, washed with 1XPBS and incubated for 1 h at room temperature with anti-rat Alex594 (1 : 500, Invitrogen, cat. #A11007). MEFs overexpressing the Dmt1 isoforms were also stained with rabbit anti-HA (1 : 400, Sigma, cat. #H6908) or mouse anti-FLAG M2 (1 : 500, Sigma, cat. #F3165). For combined Lamp-1 and Flag staining (both antibodies generated in closely related species), first anti-LAMP-1 primary and secondary were incubated. Next, after 1 h of blocking (5% NGS 0.2% triton X 1% BSA in 1XPBS) at room temperature, primary and secondary antibodies against FLAG were added. Finally, HA- or FLAG tags were visualized using secondary goat-anti-rabbit or mouse Alexa488 antibodies (Invitrogen), respectively.

All fluorescently labelled cells were counterstained with Dapi and analysed using an inverted Leica SPE confocal microscope and LEICA LAS AF LITE software, Wetzlar, Germany.

## Immunohistochemistry

For *Periodic Acid Schiff (PAS)* staining, LS174T cells with stable knockdown of *Dmt1-ire* or SCRAMBLED (SCR) were seeded on Poly-L-lysine coated coverslips. As a control, shSCR cells were treated with DMSO or DBZ for 7 days. After 7 days, cells were rinsed with 1XPBS and fixed in 4% PFA in 1XPBS for 15 min at room

temperature. After fixation, cells were incubated with periodic acid solution (Sigma, cat. #3951) for 5 min at room temperature. Next, cells were rinsed with MilliQ and stained with Schiff reagent (Sigma, cat. #3952) for 15 min at room temperature. Finally, cells were rinsed with tap water, dehydrated using 80% ethanol and mounted on glass slides using DPX mounting medium.

### Immunoblotting

Cell lysates were prepared in 1xLaemlli loading buffer. Proteins were separated on Tris-HCL SDS/PAGE gels and transferred onto PVDF membranes. Membranes were blocked in 5% dried skimmed milk (Marvel) and 0.05% Tween20 in 1XTBS. Protein detection was performed with subsequent primary antibodies: rabbit anti-cleaved Notch1 (Val 1744, D3B8) (Cell Signalling, Danvers, MA, USA; cat. #4147S, 1 : 1000), rabbit anti-lamin A (C-term) (Sigma, cat. #L1293, 1 : 1000), mouse anti-actin clone C4 (MP Biomedicals, Santa Ana, CA, USA; cat. # 691001, 1 : 20 000), mouse anti-Myc (9e10) (3 mg·mL<sup>-1</sup>, 1 : 1000), mouse anti-skeletal myosin FAST (Sigma, cat. #M4276, 1 : 1000), rabbit anti-Notch1 (C-20) (Santa Cruz, Dallas, TX, USA; cat. #sc-6014-R, 1 : 1000), rabbit anti-LC3B (MBL, WOBURN, MA, USA; cat. #PM036, 1 : 1000), mouse anti-Rab5A (Cell Signalling, cat. #46449, 1 : 1000), rabbit anti-EEA1 (Abcam, cat. #ab2900, 1 : 1000), mouse anti-vinculin (Sigma, cat. #V9131, 1 : 5000), mouse anti-FLAG M2 (Sigma, cat. #F3165, 1 : 1000), rabbit anti-HA (Sigma, cat. #H6908, 1 : 1000), rabbit anti-Dmt1 (Novus Biologicals, Centennial, CO 80112, USA; cat. #NBP2-30045, 1 : 1000), mouse anti-transferrin receptor (Invitrogen, cat. #13-6800, 1 : 1000) and rabbit anti-LAMP1 (Abcam, cat. #ab24170, 1 : 1000). Secondary antibodies used were anti-mouse (Cell Signalling, cat. #7076S, 1 : 5000) or anti-rabbit IgG-horseradish peroxidase (Cell Signalling, cat. #7074S, 1 : 5000). Amersham ECL Prime Western Blotting Detection Reagent (GE Healthcare, Chicago, IL, USA) was used for visualization as described by the manufacturer.

### Quantitative RT-PCR

Total RNA was isolated using NucleoSpin RNA (Macherey-Nagel, Düren, Germany) from cells according to the manufacturer's protocol. cDNA was obtained using iScript cDNA synthesis kit (Bio-Rad, Hercules, CA, USA) followed by SYBR-green-based reverse transcription quantitative PCR (qRT-PCR) using SensiMix SYBR high-ROX kit (GC Biotech, Waddinxveen, The Netherlands). mRNA expression was analysed using of forward and reverse primers (Tables S4 and S5). In addition, cycle threshold (C<sub>t</sub>) values were analysed with CFX Connect Real Time System (Bio-Rad) and *Csnk2a2* (mouse) and *GAPDH* (human) were used as housekeeping genes.

### Notch1 receptor flow cytometry

Notch1 receptor availability at the cell surface was analysed by flow cytometry. Dmt1 WT and KO MEFs were fixed in 4% PFA in 1XPBS and stained with a PE-labelled mouse anti-Notch1 antibody targeting the extracellular domain of Notch1 (1 : 40, BioLegend, San Diego, CA, USA; cat. #352105) for 15 min at 4 °C. For total Notch1 receptor expression, Dmt1 WT and KO MEFs were permeabilized with saponin-based permeabilization reagent (Thermo Fisher Scientific, cat. #C10418) before staining. A PE-labelled mouse IgG1κ was used as isotype control (BioLegend). After staining, cells were analysed using a FACS-CantoII cytometer with bd facsdivaBD FACSDIVA 6.1.1 software. Using FLOWV10.1, doublets and cellular debris were excluded. Mean fluorescent intensity (MFI) was determined and normalized to the control to obtain the fold change in extracellular Notch1 receptor expression.

### DMT1 isoform expression in CRC peritoneal metastases

RNA-Seq data from human colorectal cancer patients were described [36] deposited and retrieved from GEO (GSE190609). Fastq files were mapped to HG19/GRCh37 using the STAR [73] algorithm, with GENCODE-v32\_GRCh37 as annotation source. BAM files were subsequently passed to RSEM [74] for isoform quantification using GENCODE-v32\_GRCh37 as annotation source. The results were converted into a dataset in the R2: genomics analysis and visualization platform (<http://r2.amc.nl>). R2 was used for subsequent analyses and visualizations.

### Iron (Fe<sup>2+</sup>) and cytoplasmic ROS flow cytometry assay

Iron (Fe<sup>2+</sup>) was detected in Dmt1 WT and KO MEFs with the fluorescent imaging probe BioTracker 575 Red Fe<sup>2+</sup> Dye (Sigma, cat. #SCT030) according to the manufacturer's protocol. In short, cell culture media was removed, and cells were washed with 1xHBSS and subsequently stained with 5 μM BioTracker 575 Red Fe<sup>2+</sup> dye for 1 h at 37 °C. Next, cells were washed with 1xHBSS analysed by flow cytometry. Cytoplasmic ROS levels were analysed by incubating Dmt1 WT and KO MEFs [pretreated with 10 mM of N-Acetylcysteine (NAC, Sigma Aldrich) for 20 min at 37 °C in complete medium] with 5 μM of CellROX Deep Red Reagent (Thermo Fisher, cat. # C10422) in serum-free medium at 37 °C for 30 min. Fe<sup>2+</sup> and cytoplasmic ROS levels were analysed by a FACSCantoII cytometer with BD FACSDIVA 6.1.1 software. FlowJo V10.1 was used to: exclude doublets and cellular debris and analyse the mean fluorescent intensity (MFI). MFI was normalized to the DMSO control to obtain the fold change in cytoplasmic ROS levels.

## Intestinal organoid culture and lentiviral transduction

Organoids were extracted from 8-week-old *Villin-Cre* and the *Villin-Cre-Apc<sup>lox/lox</sup>* mice (The Jackson Laboratory, Bar Harbor, Maine, USA) treated with four daily injections of 2 mg tamoxifen in sunflower oil intraperitoneally. Mice were sacrificed 14 days after the last injection. All animal experiments were ethically approved and conducted according to regulations at the University of Liege. Organoid extraction was performed as described previously [75,76]. Briefly, small pieces of intestine were incubated in 2 mM EDTA-PBS for 30 min at 4 °C. Crypts were extracted, washed twice in PBS and cultured at the same density in Matrigel (BD). WT organoids were grown in IntestiCult™ Organoid Growth Medium (StemCell). *Apc* organoids were grown in DMEM/F12 supplemented with B27, N2, EGF (20 ng·mL<sup>-1</sup>) and Noggin (100 ng·mL<sup>-1</sup>).

The shRNA sequences targeting *Dmt1-ire*, *Dmt1+ire* or scrambled (Scr) control were inserted into a pLKO1-puro vector. Lentiviral particles were generated by co-transfection of the pLKO1-puro plasmids with packaging plasmid psPAX2 and the envelope plasmid pMD2.G (VSV-G) into Hek293T cells using Lipofectamine (Thermo Fisher). Intestinal stem cells were enriched by valproic acid and CHIR99021 treatment [77]. They were incubated overnight with lentiviral supernatants, after which stably transduced cells were selected by 72 h puromycin (1 µg·mL<sup>-1</sup>) selection and grown in organoids using IntestiCult™ Organoid Growth Medium (Mouse) (STEMCELL Technologies, Vancouver, CAN; cat. #06005). Organoids were dissociated and replated every 10–14 days. Organoids were derived from wild-type mice ( $n = 5$ ) and from *Apc*-mutant mice ( $n = 3$ ).

## Electron microscopy

Cells were seeded in a 6-well plate at 90% confluence and left to attach overnight. Next, cells were fixed in 2.5% glutaraldehyde in 0.1 M phosphate buffer (pH 7.4) at room temperature for 1 h. After the first fixation, fresh fixative was added, and the cells were stored at 4 degrees for 24 h. Next, organoids were fixed with 1.5% glutaraldehyde in 0.1 M cacodylate buffer for 2 min at room temperature. The fixative was refreshed and kept for 24 h at 4 °C. Next, the cells/organoids were washed in 0.1 M cacodylate buffer and postfixed with 1% osmium tetroxide and 1.5% potassium ferrocyanide in cacodylate buffer for 1 h at 4 °C. Finally, the fixed cells/organoids were dehydrated in ethanol, infiltrated with Epon resin, embedded in resin and polymerized at 60 degrees for 72 h. Ultrathin sections were obtained using Ultracut UCT ultramicrotome (Leica Microsystems, Vienna, Austria) and mounted on Formvar-coated copper grids. These grids were stained with 2% uranyl acetate in 50% ethanol and lead citrate. Electron microscopic images were obtained using a Tecnai T12

electron microscope equipped with an Eagle 4kx4k CCD camera (Thermo Fisher Scientific).

## Toluidine blue staining

For toluidine blue staining, semi-thin sections (1 µm) of EM-fixed organoids were stained with 1% toluidine blue and 1% sodium tetraborate dissolved in distilled water for 30–60 s. Excess staining was rinsed with distilled water, and slides were analysed by Light Microscope Perkin Elmer Nuance FX.

## Statistical analysis

Data are presented as mean, including the standard deviation (SD) of three independent experiments. Statistical analyses were performed using GraphPad Prism 5, and statistical significance was defined as  $P$ -value < 0.05. One-way ANOVA and a Tukey post-test were used for statistical analysis (unless stated otherwise).

## Acknowledgements

We thank David Root, David Sabatini, Adam Karpf, Raphael Kopan, David Spencer, Michael Garrick, Didier Trono and Bob Weinberg for sharing reagents. We thank Matt Roush for his assistance with cell sorting and Kasper Rouschop for helpful discussions (Maastricht University). We also thank Sara Cherry, Pilar Martinez-Martinez, Ramon Langen and Marc van de Wetering for providing cell lines. We also acknowledge Carmen López Iglesias, Kèvin Knoops and Willine van de Wetering from the Microscopy CORE Lab (M4I, Maastricht University) for scientific and technical support in the electron microscopy. Lastly, we thank MSc students: Daphne Peters and Hannah Goldfarb Wittkopf for help in experiments. This work was supported by Maastricht Clinic, the European Research Council (ERC) under the European Community Seventh Framework Program (FP7/2007-2013) ERC Starting Grant 208259 and the Kootstra-Talent Fellowship Program 2016-2017 from Maastricht-UMC+ and a grant from the Netherlands Organisation of scientific research (NWO OCENW.M20.155).

## Conflicts of interest

The authors declare no conflict of interest.

## Author contributions

JH, AG, JP, FR and KK performed the experiments and analysed the experimental data. JH drafted the

manuscript and designed the figures under the supervision of AG and MV. AG, MV, FR and KK contributed to the design and implementation of the research. OK, DZ and JK performed the expression analysis on peritoneal metastases. All authors discussed the results and commented on the manuscript.

## Peer review

The peer review history for this article is available at <https://www.webofscience.com/api/gateway/wos/peer-review/10.1111/febs.16946>.

## Data availability statement

The data that support the findings of this study are available from the corresponding author ([marc.vooijs@maastrichtuniversity.nl](mailto:marc.vooijs@maastrichtuniversity.nl)) upon reasonable request.

## References

- 1 Siebel C & Lendahl U (2017) Notch signaling in development, tissue homeostasis, and disease. *Physiol Rev* **97**, 1235–1294.
- 2 Kopan R & Ilagan MXG (2009) The canonical notch signaling pathway: unfolding the activation mechanism. *Cell* **137**, 216–233.
- 3 Aster JC, Pear WS & Blacklow SC (2017) The varied roles of notch in cancer. *Annu Rev Pathol* **12**, 245–275.
- 4 Groot AJ, Cobzaru C, Weber S, Saftig P, Blobel CP, Kopan R, Vooijs M & Franzke CW (2013) Epidermal ADAM17 is dispensable for Notch activation. *J Invest Dermatol* **133**, 2286–2288.
- 5 Groot AJ, Habets R, Yahyanejad S, Hodin CM, Reiss K, Saftig P, Theys J & Vooijs M (2014) Regulated proteolysis of NOTCH2 and NOTCH3 receptors by ADAM10 and presenilins. *Mol Cell Biol* **34**, 2822–2832.
- 6 Sulis ML, Saftig P & Ferrando A (2011) Redundancy and specificity of the metalloprotease system mediating oncogenic NOTCH1 activation in T-ALL. *Leukemia* **25**, 1564–1569.
- 7 van Tetering G, van Diest P, Verlaan I, van der Wall E, Kopan R & Vooijs M (2009) Metalloprotease ADAM10 is required for Notch1 site 2 cleavage. *J Biol Chem* **284**, 31018–31027.
- 8 Pasternak SH, Bagshaw RD, Guiral M, Zhang S, Ackerley CA, Pak BJ, Callahan JW & Mahuran DJ (2003) Presenilin-1, nicastrin, amyloid precursor protein, and  $\gamma$ -secretase activity are co-localized in the lysosomal membrane. *J Biol Chem* **278**, 26687–26694.
- 9 Kaether C, Haass C & Steiner H (2006) Assembly, trafficking and function of  $\gamma$ -secretase. *Neurodegener Dis* **3**, 275–283.
- 10 Tagami S, Okochi M, Yanagida K, Ikuta A, Fukumori A, Matsumoto N, Ishizuka-Katsura Y, Nakayama T, Itoh N, Jiang J *et al.* (2008) Regulation of Notch signaling by dynamic changes in the precision of S3 cleavage of Notch-1. *Mol Cell Biol* **28**, 165–176.
- 11 Sannerud R, Esseleens C, Ejsmont P, Mattered R, Rochin L, Tharkeshwar AK, de Baets G, de Wever V, Habets R, Baert V *et al.* (2016) Restricted location of PSEN2/ $\gamma$ -secretase determines substrate specificity and generates an intracellular A $\beta$  Pool. *Cell* **166**, 193–208.
- 12 Hounjet J, Habets R, Schaaf MB, Hendrickx TC, Barbeau LM, Yahyanejad S, Rouschop KM, Groot AJ & Vooijs M (2019) The anti-malarial drug chloroquine sensitizes oncogenic NOTCH1 driven human T-ALL to  $\gamma$ -secretase inhibition. *Oncogene* **38**, 5457–5468.
- 13 Kobia F, Duchi S, Deflorian G & Vaccari T (2014) Pharmacologic inhibition of vacuolar H<sup>+</sup> ATPase reduces physiologic and oncogenic Notch signaling. *Mol Oncol* **8**, 207–220.
- 14 Schneider M, Troost T, Grawe F, Martinez-Arias A & Klein T (2013) Activation of Notch in Igd mutant cells requires the fusion of late endosomes with the lysosome. *J Cell Sci* **126**, 645–656.
- 15 Sethi N, Yan Y, Quek D, Schupbach T & Kang Y (2010) Rabconnectin-3 is a functional regulator of mammalian Notch signaling. *J Biol Chem* **285**, 34757–34764.
- 16 Vaccari T, Duchi S, Cortese K, Tacchetti C & Bilder D (2010) The vacuolar ATPase is required for physiological as well as pathological activation of the Notch receptor. *Development* **137**, 1825–1832.
- 17 Fleming MD, Trenor CC, Su MA, Foerzler D, Beier DR, Dietrich WF & Andrews NC (1997) Microcytic anaemia mice have a mutation in Nramp2, a candidate iron transporter gene. *Nat Genet* **16**, 383–386.
- 18 Su MA, Trenor CC III, Fleming JC, Fleming MD & Andrews NC (1998) The G185R mutation disrupts function of the iron transporter Nramp2. *Blood* **92**, 2157–2163.
- 19 Touret N, Martin-Orozco N, Paroutis P, Furuya W, Lam-Yuk-Tseung S, Forbes J, Gros P & Grinstein S (2004) Molecular and cellular mechanisms underlying iron transport deficiency in microcytic anemia. *Blood* **104**, 1526–1533.
- 20 Fleming MD, Romano MA, Su MA, Garrick LM, Garrick MD & Andrews NC (1998) Nramp2 is mutated in the anemic Belgrade (b) rat: evidence of a role for Nramp2 in endosomal iron transport. *Proc Natl Acad Sci USA* **95**, 1148–1153.
- 21 Lee PL, Gelbart T, West C, Halloran C & Beutler E (1998) The human Nramp2 gene: characterization of the gene structure, alternative splicing, promoter region and polymorphisms. *Blood Cells Mol Dis* **24**, 199–215.
- 22 Hubert N & Hentze MW (2002) Previously uncharacterized isoforms of divalent metal transporter

- (DMT)-1: implications for regulation and cellular function. *Proc Natl Acad Sci USA* **99**, 12345–12350.
- 23 Mackenzie B, Takanaga H, Hubert N, Rolfs A & Hediger MA (2007) Functional properties of multiple isoforms of human divalent metal-ion transporter 1 (DMT1). *Biochem J* **403**, 59–69.
  - 24 Garrick MD, Kuo H-C, Vargas F, Singleton S, Zhao L, Smith JJ, Paradkar P, Roth JA & Garrick LM (2006) Comparison of mammalian cell lines expressing distinct isoforms of divalent metal transporter 1 in a tetracycline-regulated fashion. *Biochem J* **398**, 539–546.
  - 25 Bozkulak EC & Weinmaster G (2009) Selective use of ADAM10 and ADAM17 in activation of Notch1 signaling. *Mol Cell Biol* **29**, 5679–5695.
  - 26 Hur JY, Teranishi Y, Kihara T, Yamamoto NG, Inoue M, Hosia W, Hashimoto M, Winblad B, Frykman S & Tjernberg LO (2012) Identification of novel  $\gamma$ -secretase-associated proteins in detergent-resistant membranes from brain. *J Biol Chem* **287**, 11991–12005.
  - 27 Wu ZQ, Li D, Huang Y, Chen XP, Huang W, Liu CF, Zhao HQ, Xu RX, Cheng M, Schachner M *et al.* (2017) Caspr controls the temporal specification of neural progenitor cells through Notch signaling in the developing mouse cerebral cortex. *Cereb Cortex* **27**, 1369–1385.
  - 28 Nofziger D, Miyamoto A, Lyons KM & Weinmaster G (1999) Notch signaling imposes two distinct blocks in the differentiation of C2C12 myoblasts. *Development* **126**, 1689–1702.
  - 29 Berkes CA & Tapscott SJ, eds. (2005) MyoD and the transcriptional control of myogenesis. *Semin Cell Dev Biol* **16**, 585–595.
  - 30 Franklin J, Berechid B, Cutting F, Presente A, Chambers C, Foltz DR, Ferreira A & Nye JS (1999) Autonomous and non-autonomous regulation of mammalian neurite development by Notch1 and Delta1. *Curr Biol* **9**, 1448–1457.
  - 31 van Es JH, Van Gijn ME, Riccio O, Van Den Born M, Vooijs M, Begthel H *et al.* (2005) Notch/ $\gamma$ -secretase inhibition turns proliferative cells in intestinal crypts and adenomas into goblet cells. *Nature* **435**, 959–963.
  - 32 Vooijs M, Ong C-T, Hadland B, Huppert S, Liu Z, Korving J, van den Born M, Stappenbeck T, Wu Y, Clevers H *et al.* (2007) Mapping the consequence of Notch1 proteolysis in vivo with NIP-CRE. *Development* **134**, 535–544.
  - 33 Vooijs M, Liu Z & Kopan R (2011) Notch: architect, landscaper, and guardian of the intestine. *Gastroenterology* **141**, 448–459.
  - 34 Yang Y, Zhu R, Bai J, Zhang X, Tian Y, Li X, Peng Z, He Y, Chen L, Ji Q *et al.* (2011) Numb modulates intestinal epithelial cells toward goblet cell phenotype by inhibiting the Notch signaling pathway. *Exp Cell Res* **317**, 1640–1648.
  - 35 Milano J, McKay J, Dagenais C, Foster-Brown L, Pognan F, Gadiant R, Jacobs RT, Zacco A, Greenberg B & Ciaccio PJ (2004) Modulation of Notch processing by  $\gamma$ -secretase inhibitors causes intestinal goblet cell metaplasia and induction of genes known to specify gut secretory lineage differentiation. *Toxicol Sci* **82**, 341–358.
  - 36 Laoukili J, Constantinides A, Wassenaar ECE, Elias SG, Raats DAE, van Schelven SJ, van Wettum J, Volckmann R, Koster J, Huitema ADR *et al.* (2022) Peritoneal metastases from colorectal cancer belong to consensus molecular subtype 4 and are sensitised to oxaliplatin by inhibiting reducing capacity. *Br J Cancer* **126**, 1824–1833.
  - 37 Radulescu S, Brookes MJ, Salgueiro P, Ridgway RA, McGhee E, Anderson K, Ford SJ, Stones DH, Iqbal TH, Tselepis C *et al.* (2012) Luminal iron levels govern intestinal tumorigenesis after Apc loss in vivo. *Cell Rep* **2**, 270–282.
  - 38 Turcu AL, Versini A, Khene N, Gaillet C, Cañeque T, Müller S & Rodriguez R (2020) DMT1 inhibitors kill cancer stem cells by blocking lysosomal iron translocation. *Chemistry* **26**, 7369–7373.
  - 39 Lewis C, Graves S, Cai W, Nickles R, Meyerand M & Suzuki M (2014) DMT1, a novel PET/MR reporter protein for neural stem cell tracking. *J Nucl Med* **55** (Suppl 1), 60.
  - 40 Han Z, Yu Y, Xu J, Bao Z, Xu Z, Hu J, Yu M, Bamba D, Ma W, Ding F *et al.* (2019) Iron homeostasis determines fate of human pluripotent stem cells via glycerophospholipids-epigenetic circuit. *Stem Cells* **37**, 489–503.
  - 41 Švec J, Štastná M, Janečková L, Hrkulák D, Vojtěchová M, Onhajzer J, Kříž V, Galušková K, Šloncová E, Kubovčíak J *et al.* (2022) TROP2 represents a negative prognostic factor in colorectal adenocarcinoma and its expression is associated with features of epithelial–mesenchymal transition and invasiveness. *Cancer* **14**, 4137.
  - 42 Ohmachi T, Tanaka F, Mimori K, Inoue H, Yanaga K & Mori M (2006) Clinical significance of TROP2 expression in colorectal cancer. *Clin Cancer Res* **12**, 3057–3063.
  - 43 Vooijs M, Schroeter EH, Pan Y, Blandford M & Kopan R (2004) Ectodomain shedding and intramembrane cleavage of mammalian Notch proteins are not regulated through oligomerization. *J Biol Chem* **279**, 50864–50873.
  - 44 Chaumet A, Wright GD, Seet SH, Tham KM, Gounko NV & Bard F (2015) Nuclear envelope-associated endosomes deliver surface proteins to the nucleus. *Nat Commun* **6**, 8218.
  - 45 Papadopoulos C & Meyer H (2017) Detection and clearance of damaged lysosomes by the endo-lysosomal damage response and lysophagy. *Curr Biol* **27**, R1330–R1341.

- 46 Kurz T, Terman A, Gustafsson B & Brunk UT (2008) Lysosomes in iron metabolism, ageing and apoptosis. *Histochem Cell Biol* **129**, 389–406.
- 47 Small SA & Gandy S (2006) Sorting through the cell biology of Alzheimer's disease: intracellular pathways to pathogenesis. *Neuron* **52**, 15–31.
- 48 Marshansky V & Futai M (2008) The V-type H<sup>+</sup>-ATPase in vesicular trafficking: targeting, regulation and function. *Curr Opin Cell Biol* **20**, 415–426.
- 49 Yan Y, Deneff N & Schüpbach T (2009) The vacuolar proton pump, V-ATPase, is required for Notch signaling and endosomal trafficking in drosophila. *Dev Cell* **17**, 387–402.
- 50 Paul MK, Bisht B, Darmawan DO, Chiou R, Ha VL, Wallace WD, Chon AT, Hegab AE, Grogan T, Elashoff DA *et al.* (2014) Dynamic changes in intracellular ROS levels regulate airway basal stem cell homeostasis through Nrf2-dependent Notch signaling. *Cell Stem Cell* **15**, 199–214.
- 51 Tabuchi M, Tanaka N, Nishida-Kitayama J, Ohno H & Kishi F (2002) Alternative splicing regulates the subcellular localization of divalent metal transporter 1 isoforms. *Mol Biol Cell* **13**, 4371–4387.
- 52 Lam-Yuk-Tseung S & Gros P (2006) Distinct targeting and recycling properties of two isoforms of the iron transporter DMT1 (NRAMP2, Slc11A2). *Biochemistry* **45**, 2294–2301.
- 53 Tabuchi M, Yoshimori T, Yamaguchi K, Yoshida T & Kishi F (2000) Human NRAMP2/DMT1, which mediates iron transport across endosomal membranes, is localized to late endosomes and lysosomes in HEP-2 cells. *J Biol Chem* **275**, 22220–22228.
- 54 Yamamoto S, Charng W-L & Bellen HJ (2010) Endocytosis and intracellular trafficking of Notch and its ligands. *Curr Top Dev Biol* **92**, 165–200.
- 55 Khwaja SS, Liu H, Tong C, Jin F, Pear WS, Van Deursen J & Bram RJ (2010) HIV-1 rev-binding protein accelerates cellular uptake of iron to drive Notch-induced T cell leukemogenesis in mice. *J Clin Invest* **120**, 2537–2548.
- 56 Jiang XP, Elliott RL & Head JF (2010) Manipulation of iron transporter genes results in the suppression of human and mouse mammary adenocarcinomas. *Anticancer Res* **30**, 759–765.
- 57 Shawki A, Anthony SR, Nose Y, Engevik MA, Niespodzany EJ, Barrientos T, Öhrvik H, Worrell RT, Thiele DJ & Mackenzie B (2015) Intestinal DMT1 is critical for iron absorption in the mouse but is not required for the absorption of copper or manganese. *Am J Physiol Gastrointest Liver Physiol* **309**, G635–G647.
- 58 Mumm JS, Schroeter EH, Saxena MT, Griesemer A, Tian X, Pan DJ, Ray WJ & Kopan R (2000) A ligand-induced extracellular cleavage regulates gamma-secretase-like proteolytic activation of Notch1. *Mol Cell* **5**, 197–206.
- 59 Gerber H, Wu F, Dimitrov M, Osuna GMG & Fraering PC (2017) Zinc and copper differentially modulate amyloid precursor protein processing by  $\gamma$ -secretase and amyloid- $\beta$  peptide production. *J Biol Chem* **292**, 3751–3767.
- 60 Xue X, Ramakrishnan SK, Weisz K, Triner D, Xie L, Attili D, Pant A, Györfy B, Zhan M, Carter-Su C *et al.* (2016) Iron uptake via DMT1 integrates cell cycle with JAK-STAT3 signaling to promote colorectal tumorigenesis. *Cell Metab* **24**, 447–461.
- 61 Moffat J, Grueneberg DA, Yang X, Kim SY, Kloepper AM, Hinkle G, Piqani B, Eisenhaure TM, Luo B, Grenier JK *et al.* (2006) A lentiviral RNAi library for human and mouse genes applied to an arrayed viral high-content screen. *Cell* **124**, 1283–1298.
- 62 Sarbassov DD, Guertin DA, Ali SM & Sabatini DM (2005) Phosphorylation and regulation of Akt/PKB by the rictor-mTOR complex. *Science* **307**, 1098–1101.
- 63 Barger CJ, Branick C, Chee L & Karpf AR (2019) Pan-cancer analyses reveal genomic features of FOXM1 overexpression in cancer. *Cancer* **11**, 251.
- 64 Ong C-T, Cheng H-T, Chang L-W, Ohtsuka T, Kageyama R, Stormo GD & Kopan R (2006) Target selectivity of vertebrate Notch proteins collaboration between discrete domains and CSL-binding site architecture determines activation probability. *J Biol Chem* **281**, 5106–5119.
- 65 Shahi P, Seethammagari MR, Valdez JM, Xin L & Spencer DM (2011) Wnt and Notch pathways have interrelated opposing roles on prostate progenitor cell proliferation and differentiation. *Stem Cells* **29**, 678–688.
- 66 Garrick MD, Zhao L, Roth JA, Jiang H, Feng J, Foot NJ, Dalton H, Kumar S & Garrick LM (2012) Isoform specific regulation of divalent metal (ion) transporter (DMT1) by proteasomal degradation. *Biometals* **25**, 787–793.
- 67 Dull T, Zufferey R, Kelly M, Mandel R, Nguyen M, Trono D & Naldini L (1998) A third-generation lentivirus vector with a conditional packaging system. *J Virol* **72**, 8463–8471.
- 68 Stewart SA, Dykxhoorn DM, Palliser D, Mizuno H, Yu EY, An DS, Sabatini DM, Chen IS, Hahn WC, Sharp PA *et al.* (2003) Lentivirus-delivered stable gene silencing by RNAi in primary cells. *RNA* **9**, 493–501.
- 69 Rose PP, Hanna SL, Spiridigliozzi A, Wannissorn N, Beiting DP, Ross SR, Hardy RW, Bambina SA, Heise MT & Cherry S (2011) Natural resistance-associated macrophage protein is a cellular receptor for sindbis virus in both insect and mammalian hosts. *Cell Host Microbe* **10**, 97–104.
- 70 Fiddes IT, Lodewijk GA, Mooring M, Bosworth CM, Ewing AD, Mantalas GL, Novak AM, van den Bout A, Bishara A, Rosenkrantz JL *et al.* (2018) Human-specific NOTCH2NL genes affect Notch signaling and cortical neurogenesis. *Cell* **173**, 1356–1369.e22.

- 71 Foot NJ, Dalton HE, Shearwin-Whyatt LM, Dorstyn L, Tan S-S, Yang B & Kumar S (2008) Regulation of the divalent metal ion transporter DMT1 and iron homeostasis by a ubiquitin-dependent mechanism involving Ndfips and WWP2. *Blood* **112**, 4268–4275.
- 72 Langen RC, Schols AM, Kelders MC, Wouters EF & Janssen-Heininger YM (2003) Enhanced myogenic differentiation by extracellular matrix is regulated at the early stages of myogenesis. *In Vitro Cell Dev Biol Anim* **39**, 163–169.
- 73 Dobin A, Davis CA, Schlesinger F, Drenkow J, Zaleski C, Jha S, Batut P, Chaisson M & Gingeras TR (2013) STAR: ultrafast universal RNA-seq aligner. *Bioinformatics* **29**, 15–21.
- 74 Li B & Dewey CN (2011) RSEM: accurate transcript quantification from RNA-Seq data with or without a reference genome. *BMC Bioinformatics* **12**, 323.
- 75 Barker N, van Es JH, Kuipers J, Kujala P, van den Born M, Cozijnsen M, Haegbarth A, Korving J, Begthel H, Peters PJ *et al.* (2007) Identification of stem cells in small intestine and colon by marker gene Lgr5. *Nature* **449**, 1003–1007.
- 76 Ladang A, Rapino F, Heukamp LC, Tharun L, Shostak K, Hermand D, Delaunay S, Klevernic I, Jiang Z, Jacques N *et al.* (2015) Elp3 drives Wnt-dependent tumor initiation and regeneration in the intestine. *J Exp Med* **212**, 2057–2075.
- 77 Yin X, Farin HF, van Es JH, Clevers H, Langer R & Karp JM (2014) Niche-independent high-purity cultures

of Lgr5+ intestinal stem cells and their progeny. *Nat Methods* **11**, 106–112.

## Supporting information

Additional supporting information may be found online in the Supporting Information section at the end of the article.

**Table S1.** Pathway analysis shRNA screen.

**Table S2.** Correlation analysis of log<sub>2</sub> ratio Dmt-Ire/+Ire and Notch target gene expression.

**Table S3.** Targeting sequences of shRNAs.

**Table S4.** Mouse qRT-PCR primer sequences.

**Table S5.** Human qRT-PCR primer sequences.

**Fig. S1.** Loss of Dmt1 results in decreased Notch signalling.

**Fig. S2.** Ectopic activation of Notch1 rescues loss of Notch signalling in Dmt1 KO MEFs.

**Fig. S3.** Dmt1 controls Notch1 signalling in an isoform-dependent manner.

**Fig. S4.** Dmt1 isoform expression in cell lines and mouse intestinal organoids.

**Fig. S5.** Loss of APC in intestinal organoids results in diminished differentiation correlating with Dmt1 in human colorectal cancer.